Spatial and single-cell colocalisation analysis reveals MDK-mediated immunosuppressive environment with regulatory T cells in colorectal carcinogenesis

Masahiro Hashimoto,[a,b] Yasuhiro Kojima,[c] Takeharu Sakamoto,[d,***] Yuki Ozato,[a,b] Yusuke Nakano,[a,b] Tadashi Abe,[a] Kiyotaka Hosoda,[a] Hideyuki Saito,[a,e] Satoshi Higuchi,[a,b] Yuichi Hisamatsu,[a] Takeo Toshima,[a] Yusuke Yonemura,[a] Takaaki Masuda,[a] Tsuyoshi Hata,[b] Satoshi Nagayama,[f] Koichi Kagawa,[g] Yasuhiro Goto,[g] Mitsuaki Utou,[h] Ayako Gamachi,[i] Kiyomi Imamura,[j] Yuta Kuze,[j] Junko Zenkoh,[j] Ayako Suzuki,[j] Kazuki Takahashi,[k] Atsushi Niida,[k] Haruka Hirose,[l] Shuto Hayashi,[l] Jun Koseki,[l] Satoshi Fukuchi,[m] Kazunari Murakami,[n] Tomoharu Yoshizumi,[o] Kenji Kadomatsu,[p] Taro Tobo,[h] Yoshinao Oda,[q] Mamoru Uemura,[b] Hidetoshi Eguchi,[b] Yuichiro Doki,[b] Masaki Mori,[r] Masanobu Oshima,[s] Tatsuhiro Shibata,[k] Yutaka Suzuki,[j] Teppei Shimamura,[l,t,**] and Koshi Mimori[a,u,*]

[a]Department of Surgery, Kyushu University Beppu Hospital, Beppu, 874-0838, Japan
[b]Department of Gastroenterological Surgery, Osaka University Graduate School of Medicine, Suita, 565-0871, Japan
[c]Division of Computational Bioscience, National Cancer Center Research Institute, Tokyo, 104-0045, Japan
[d]Department of Cancer Biology, Institute of Biomedical Science, Kansai Medical University, Hirakata, 573-1010, Japan
[e]Department of General Surgical Science, Gastroenterological Surgery, Gunma University Graduate School of Medicine, Maebashi, 371-8511, Japan
[f]Department of Surgery, Uji-Tokushukai Medical Center, Uji, 611-0041, Japan
[g]Department of Gastroenterology, Shin Beppu Hospital, Beppu, 874-8538, Japan
[h]Department of Pathology, Kyushu University Beppu Hospital, Beppu, 874-0838, Japan
[i]Department of Pathology, Oita Oka Hospital, Oita, 870-0192, Japan
[j]Laboratory of Systems Genomics, Department of Computational Biology and Medical Sciences, Graduate School of Frontier Sciences, The University of Tokyo, Kashiwa, 277-8561, Japan
[k]Laboratory of Molecular Medicine, Human Genome Center, The Institute of Medical Science, The University of Tokyo, Tokyo, 108-8639, Japan
[l]Division of Systems Biology, Nagoya University Graduate School of Medicine, Nagoya, 466-8550, Japan
[m]Department of Gastroenterological Medicine, Almeida Memorial Hospital, Oita, 870-1195, Japan
[n]Department of Gastroenterology, Oita University Hospital, Yufu, 879-5593, Japan
[o]Department of Surgery and Science, Graduate School of Medical Sciences, Kyushu University, Fukuoka, 812-8582, Japan
[p]Department of Biochemistry, Nagoya University Graduate School of Medicine, Nagoya, 466-8550, Japan
[q]Department of Anatomic Pathology, Kyushu University Hospital, Fukuoka, 812-8582, Japan
[r]Tokai University School of Medicine, Isehara, 259-1193, Japan
[s]Division of Genetics, Cancer Research Institute, Kanazawa University, Kanazawa, 920-1192, Japan
[t]Department of Computational and Systems Biology, Medical Research Insitute, Tokyo Medical and Dental University, Bunkyo-ku, Tokyo 113-0034, Japan

eBioMedicine
2024;103: 105102
Published Online 12 April 2024
https://doi.org/10.1016/j.ebiom.2024.105102

Summary

Background Cell–cell interaction factors that facilitate the progression of adenoma to sporadic colorectal cancer (CRC) remain unclear, thereby hindering patient survival.

Methods We performed spatial transcriptomics on five early CRC cases, which included adenoma and carcinoma, and one advanced CRC. To elucidate cell–cell interactions within the tumour microenvironment (TME), we investigated the colocalisation network at single-cell resolution using a deep generative model for colocalisation analysis, combined with a single-cell transcriptome, and assessed the clinical significance in CRC patients.

Findings CRC cells colocalised with regulatory T cells (Tregs) at the adenoma–carcinoma interface. At early-stage carcinogenesis, cell–cell interaction inference between colocalised adenoma and cancer epithelial cells and Tregs

*Corresponding author. Department of Surgery, Kyushu University Beppu Hospital, 4546 Tsurumihara, Oaza-Tsurumi, Beppu City, Oita Prefecture, Beppu, Japan.
**Corresponding author. Division of Systems Biology, Nagoya university Graduate School of Medicine, 65 Tsurumai-cho, Showa-ku, Nagoya-shi, Aichi, Nagoya, Japan.
***Corresponding author. Department of Cancer Biology, Institute of Biomedical Science, Kansai Medical University, Hirakata, Japan.
E-mail addresses: mimori.koshi.791@m.kyushu-u.ac.jp (K. Mimori), shimamura@med.nagoya-u.ac.jp (T. Shimamura), sakamott@hirakata.kmu.ac.jp (T. Sakamoto).
[u]Lead contact.

based on the spatial distribution of single cells highlighted midkine (MDK) as a prominent signalling molecule sent from tumour epithelial cells to Tregs. Interaction between MDK-high CRC cells and SPP1+ macrophages and stromal cells proved to be the mechanism underlying immunosuppression in the TME. Additionally, we identified syndecan4 (SDC4) as a receptor for MDK associated with Treg colocalisation. Finally, clinical analysis using CRC datasets indicated that increased MDK/SDC4 levels correlated with poor overall survival in CRC patients.

Interpretation MDK is involved in the immune tolerance shown by Tregs to tumour growth. MDK-mediated formation of the TME could be a potential target for early diagnosis and treatment of CRC.

Funding Japan Society for the Promotion of Science (JSPS) Grant-in-Aid for Science Research; OITA Cancer Research Foundation; AMED under Grant Number; Japan Science and Technology Agency (JST); Takeda Science Foundation; The Princess Takamatsu Cancer Research Fund.

Keywords: MDK; Colorectal cancer; Immune tolerance; Spatial transcriptomics; Single-cell RNA sequencing; SDC4

Research in context

Evidence before this study

CRC is one of the most common cancers worldwide. The adenoma-carcinoma sequence is the established model of cancer progression in sporadic CRC. Although immunotherapy has emerged as a novel therapeutic arm, the fact that most patients with CRC do not benefit from this treatment reveals the need for a more detailed understanding of the mechanisms underlying immunosuppression in the TME. The previous reports in single-cell RNA sequencing analysis have shown that the proportion of Tregs and precancer-associated fibroblasts increases during late-stage adenoma in trajectory analysis. However, the key mediators of immune tolerance which facilitate the progression of adenoma to carcinoma remain unclear. Moreover, most previous works profiling genetic, epigenetic, and transcriptomic changes that occur in malignancy have focused on advanced tumours rather than premalignant lesions.

Added value of this study

Our integration of single-cell RNA sequencing and spatial transcriptomics of CRC at a single-cell resolution revealed that an MDK-mediated colocalisation network involving epithelial tumour cells and Tregs may induce immune tolerance in precancerous CRC tissues. In addition, examination of cell–cell interactions enabled us to identify SDC4 as a MDK receptor on Tregs. In vitro analyses using MDK-knockdown CRC cells and SDC4-knockdown Treg-like cells showed that MDK-SDC4 interaction promoted the migration of Treg-like cells. Clinically, MDK expression in early-stage CRC tissues is higher compared to that in normal tissues, and high MDK and SDC4 expression levels have been linked to poor survival in CRC patients.

Implications of all the available evidence

In this study, we simultaneously conducted a spatial transcriptome analysis as well as a single-cell RNA analysis to decipher colocalised cells and the molecular crosstalk between them via a deep-learning computational framework. Our current analysis further disclosed that MDK is involved in the immune tolerance of Tregs during the early stages of CRC, highlighting that MDK signalling may be a therapeutic target of immunotherapy aimed at CRC.

Introduction

Colorectal cancer (CRC) is the third most common cancer worldwide, with sporadic types accounting for approximately 65% of cases.[1,2] Although various therapies, such as molecular target therapy, have been developed for sporadic CRC, it remains a serious challenge with a high fatality rate and morbidity; therefore, new therapeutic approaches are needed to improve prognosis. The adenoma–carcinoma sequence is the established model of cancer progression in sporadic CRC. Approximately 80–90% of colorectal tumours are defective in adenomatous polyposis coli (*APC*), and intestinal hyperplasia is driven by the stabilisation of β-catenin and the activation of Wnt signaling.[3–9] Any subsequent carcinogenesis is triggered through the activation of mutations of the *KRAS* (or *BRAF*) oncogene and inactivation of mutations of the *TP53* tumour suppressor gene.[10,11] Although several attempts to devise molecular therapies targeting adenocarcinoma-related genes, such as *KRAS* and *MYC*, and those encoding other transcription factors, have been made, direct targeting of such genes in cancer cells has been challenging. Therefore, different cancer cells, such as immune tolerance-related cells, cancer-associated fibroblasts (CAFs), tumour-associated macrophages (TAMs), and other interstitial cells, should be considered as novel targets for cancer eradication. The effects exerted by the tumour microenvironment (TME) on carcinogenesis

remain unclear, resulting in a lack of progress in devising therapies aimed at the TME.

Previously, focusing on the genomic evolution of cancers, we multi-sampled early and advanced CRC, including carcinoma in adenoma expressed in the evolutionary model of biology, to elucidate the establishment of intratumour heterogeneity. During the progression of a precancerous lesion to carcinoma, the lesion positively selects driver mutations contributing to cancer development in a manner similar to Darwinian evolution; the TME exerts evolutionary selection pressure once driver mutations have ubiquitously evolved in a process resembling neutral evolution.[12,13] However, the role played by the TME, with particular reference to immune tolerance-related cells in the carcinogenic evolution of precancerous lesions, remains unknown. Thus, the identification of critical cell–cell interactions and genes involved in crosstalk in the TME, which exacerbate the carcinogenic process in epithelial cells may be deemed essential.

Immunotherapy, mainly using immune checkpoint inhibitors, has emerged as the fourth therapeutic arm for cancer, with high positive outcomes in specific cancers. Although treatment of sporadic CRC cases with PD-1 inhibitors, such as pembrolizumab and nivolumab, has not been successful, a significant response to dostarlimab in rectal cancer has been reported.[14] Comprehension of immune tolerance in the TME at the single-cell level may provide clues that would help better understanding the differences between treatment outcomes.[15,16]

Single-cell RNA sequencing (scRNA-seq) has contributed greatly to the elucidation of the TME in many cancers.[17–19] By integrating scRNA-seq and spatial transcriptome sequence (ST-seq) analyses, we had previously found that HLA-G secreted by malignant epithelial cells induces immune tolerance by recruiting SPP1+ macrophages to the invasive front in advanced cancer.[20] However, immune tolerance during the progression of adenoma to carcinoma remains unclear. Although scRNA-seq aimed at adenomas and carcinomas has been reported previously, this is the first study to scrutinise them in identical specimens. Furthermore, we were able to overcome sampling difficulties in adenoma and carcinoma in situ using scRNA-seq or ST-seq. Having gained patient understanding of the ethical issues involved, we obtained approval from the Kyushu University Ethics Committee for this analysis.[21,22] The use of trajectory analysis has revealed that the proportion of regulatory T cells (Tregs) and precancer-associated fibroblasts increases during late adenoma.[22] However, key mediators of cellular changes and cell–cell interactions that occur during the progression from normal to precancerous lesions to cancer remain unknown.

Herein, we focused on early-stage cancer lesions pathologically diagnosed as carcinoma in adenoma and analysed them using a deep-learning framework, DeepCOLOR.[23] Using scRNA-seq data for a reference cell population, each spot in spatial data containing multiple cells can be deconvolved to identify colocalisation networks that exist among single cells in the spatial niche. Furthermore, the spatial distribution of single cells and their gene-expression profiles may be utilised to reconstruct spatial gene-expression patterns. Our integration of scRNA-seq of CRC and ST-seq analysis of adenocarcinoma tissues enabled us to investigate immune tolerance and TME at the adenoma–tumour interface. We identified that midkine (MDK) induces Tregs in the early stage of carcinogenesis. Epithelial cells with high MDK expression colocalised with Tregs and acted on SPP1+ macrophages and fibroblasts to form the TME. Here, we show the mechanism underlying the acquisition of immune tolerance and its regulation during the development of sporadic CRC.

Methods

Experimental methods

Patient and tissue samples

CRC and normal colon tissue samples were collected according to protocols approved by the Institutional Review Board of Kyusyu University. Six samples—two fresh-frozen tissue specimens and four paraffin-embedded specimens from patients undergoing endoscopic treatment or surgery at Kyusyu University Beppu Hospital—were used for spatial transcriptomics. Surplus tumour specimens of optimal size were flash-frozen in optimal cutting temperature compound (OCT; Tissue-Tek, Sakura Finetek USA, Inc., Torrance, CA) or in 10% formalin (Sigma–Aldrich, St. Louis, MO, USA). Specimens embedded in the OCT compound were stored at –80 °C until needed. Specimens embedded in formalin were stored at room temperature until needed. All diagnoses were confirmed following histological examination by a board-certified colorectal pathologist. The four paraffin-embedded specimens, involved previously treated cases with a histologic diagnosis of adenoma and carcinoma in situ and cancer cells only in the epithelium or mucosal intrinsic layer without vascular invasion. Detailed information regarding the samples is provided (Supplementary Data 1). Informed consent was obtained in the form of an opt-out option available on the website (https://www.beppu.kyushu-u.ac.jp/geka/information/clinical_disclosure/). Those who opted out were excluded.

CRC cohort data for 137 patients who underwent surgical resection of a primary tumour at Kyusyu University Beppu Hospital (or affiliated hospitals) from 1994 to 2002 were used. Their clinicopathological factors and clinical stage were classified using the American Joint Committee on Cancer 8th edition TNM staging system. Written informed consent was obtained from all patients. Resected tumour tissues and paired normal tissues were obtained as previously described.[24]

Spatial transcriptomics

Formalin-fixed, paraffin-embedded (FFPE) samples, which had passed RNA quality control, were used for spatial transcriptomic construction and sequencing. Five-micrometer thick sections were prepared from the FFPE samples and processed using a Visium Spatial Gene Expression Slide Kit (10× Genomics) according to Visium Spatial Gene Expression Reagent Kits for FFPE User Guide. Sections were stained with H&E and imaged, followed by probe hybridisation and ligation. The captured probe library was sequenced using an MGI DNBSEQ-G400 system for 28, 10, 10, and 50 cycles for Read 1, i7, i5, and Read 2 sequences, respectively. Reads were demultiplexed and mapped to the reference genome, GRCh38 (build 2020-A, 10× Genomics), using Space Ranger software v.1.3.1 (10× Genomics). Spots were annotated by a specialist colorectal pathologist using Loupe v.6.0.0 software (10× Genomics). Spatial transcriptomics (10× Genomics Visium) for fresh-frozen specimens was performed as previously described.[20]

RT-quantitative PCR

qPCR was performed using LightCycler FastStart DNA Master SYBR Green I (Roche Diagnostics) as previously described.[25] MDK mRNA levels were normalised to those of 18 S mRNA as an internal control and expressed relative to cDNA expression from Human Universal Reference Total RNA (Clontech). The qPCR primer sequences were as follows: MDK, forward 5′-TG GAGCCGACTGCAAATACAA-3′ and reverse 5′-GGC TTAGTCACGCGGATGG-3′; SDC4, forward 5′-GAGC CCTACCAGACGATGAG-3′ and reverse 5′-GGGCC GATCATGGAGTCTTC-3′; and 18 S, forward 5′-AGTC CCTGCCCTTTGTACACA-3′ and reverse 5′-CGATCC-GAGGGCCTCACTA-3′.

Immunohistochemistry

Immunohistochemistry (IHC) was performed on FFPE CRC samples obtained from patients who underwent surgery at the Kyusyu University Beppu Hospital as previously described.[25,26] IHC was performed using rabbit monoclonal antibody (anti-Midkine; RRID:AB_880698, ab52637, 1:50, Abcam), mouse monoclonal antibody (anti-FOXP3; RRID:AB_449304, ab450, 1:100, Abcam), and rabbit polyclonal antibody (anti-SDC4; RRID:AB_2877797, 11820-1-AP, 1:200, Proteintech). FFPE cell line pellets known to express each antigen were used to establish optimal conditions, sensitivity, and specificity for immunostaining. Stained section images were captured using a Nikon camera (DS L3) (Tokyo, Japan).

Immunofluorescence analysis

Immunofluorescence analysis was performed using the following primary antibodies: anti-MDK (RRID:AB_627949, sc-46701, 1:50, Santa Cruz), anti-FOXP3 (RRID:AB_449304, ab450, 1:100, Abcam), and anti-SDC4 (RRID:AB_2877797, 11820-1-AP, 1:200, Proteintech). Next, antibodies against MDK/FOXP3 (anti-mouse IgG 488, RRID:AB_10694704, Cell Signaling) and SDC4 (anti-rabbit IgG 555, RRID:AB_10694110, Cell Signaling) were used to stain MDK/FOXP3 protein and SDC4 protein, respectively, in FFPE at a dilution of 1:500 and 1:1000, as described above, followed by the observation of fluorescent images using a fluorescence microscope (BZ-X700, Keyence, Osaka, Japan).

Cell culture

Mouse colon cancer MC-38 cells were purchased from Kerafast (Boston, MA, USA). Human colorectal cancer RKO cells were obtained from the American Type Culture Collection (Manassas, VA, USA). Human regulatory T cell-like MT-2 cells[27] were obtained from the Japanese Collection of Research Bioresources Cell Bank (Osaka, Japan). Authenticated cells obtained from cell banks were frozen immediately, thawed, and used in this study without exceeding 10 passages. MC-38 cells were cultured in Dulbecco's modified Eagle medium (FUJIFILM Wako, Osaka, Japan) and RKO and MT-2 cells were cultured in RPMI 1640 medium (FUJIFILM Wako, Osaka, Japan). All media were supplemented with 10% foetal bovine serum (FBS), 100 units/ml penicillin, and 100 μg/ml streptomycin at 37 °C in a humidified 5% CO_2 incubator. Cell lines were routinely tested for mycoplasma contamination.

Construction of the lentiviral Mdk expression vector

Mouse Mdk cDNA from mouse brain was amplified using RT-PCR and subcloned into pENTR/D-TOPO (Thermo Fisher Scientific, Waltham, MA, USA) before being transferred into the lentivirus vector pLenti6 (Thermo Fisher Scientific), as described previously.[28] Lentiviral vectors were generated and used according to the manufacturer's instructions and transfected into MC-38 cells.

siRNA knockdown

siRNAs for negative control (SIC002, MISSION siRNA Universal Negative Control #1), MDK (SASI_Hs01_00172415), and SDC4 (SASI_Hs01_00138116) were purchased from Sigma–Aldrich (St. Louis, MO, USA). siRNAs were transfected to cells at 20 nM using lipofectamine RNAiMAX (Thermo Fisher Scientific, Waltham, MA, USA). Cells were used for the indicated assays 72 h after transfection.

Western blotting

Cells were lysed in lysis buffer (1% Nonidet P-40, 50 mM Tris pH 8.0, and 150 mM NaCl) and centrifuged at 20,000 × *g* for 15 min at 4 °C. The supernatant was collected; the total protein content was measured using the Bradford assay (Bio-Rad, Hercules, CA, USA).

Proteins in the lysates were resolved using sodium dodecyl sulphate-polyacrylamide gel electrophoresis, transferred onto polyvinylidene fluoride membranes, and analysed via western blotting with mouse anti-β-actin antibody (RRID:AB_2223041, MAB1501; Merck Millipore, Burlington, MA), rabbit anti-MDK polyclonal antibody (RRID:AB_2881168, 28546-1-AP; Proteintech, Rosemont, IL, USA), or rabbit anti-SDC4 polyclonal antibody (RRID:AB_805586, NB110-41551; Novus Biologicals, Centennial, CO, USA) as primary antibodies and horse anti-mouse IgG HRP-linked antibody (RRID:AB_330924, 7076; Cell Signaling Technology, Danvers, MA, USA) and goat anti-rabbit IgG HRP-linked antibody (RRID:AB_2099233, 7074; Cell Signaling Technology) as secondary antibodies. The specificity of antibodies was confirmed by knockout/knockdown experiments of each antigen.

Tumour growth assay

MC-38 cell tumourigenicity was examined using 8-week-old male C57BL/6J mice (Clea Japan, Tokyo, Japan) and BALB/c nude mice (Clea Japan), as previously described.[29] Mice were housed at the Kansai Medical University, which is a 12:12 light:dark cycled, temperature and humidity-controlled, specific pathogen-free animal facility and with ad libitum access to food and water. Briefly, mice were randomised and 5×10^5 MC-38 cells were injected subcutaneously into the dorsal side of mice. Subsequently, implanted tumours were measured with calipers on the indicated days by a researcher in a blinded manner and mice were sacrificed 3 weeks after injection. Their volumes were calculated using the formula $V= (L \times W^2)/2$, where V is the volume (mm^3), L is the largest tumour diameter (mm), and W is the smallest tumour diameter (mm). Sample sizes of all animal experiments were predetermined. Experimental protocols were approved by the Animal Care and Use Committees of the Kansai Medical University and all experiments were conducted in accordance with the institutional ethical guidelines for animal experiments and the safety guidelines for gene manipulation experiments.

Flow cytometry

For Treg analysis, tumours were digested using a gentleMACS Dissociator and Tumour dissociation kit (Miltenyi Biotec, Bergisch Gladbach, Germany), while red blood cells were lysed with 1 × RBC Lysis Buffer (BioLegend, San Diego, CA, USA). Per sample, 2×10^6 cells in the FCM buffer (PBS containing 5% FBS and 2 mM EDTA) were treated with anti-mouse CD16/32 antibodies (RRID:AB_467134, 14-0161-85; ThermoFisher Scientific) for 30 min at 4 °C and stained with anti-mouse CD45 PE-Cy7 (RRID:AB_2734986, 25-0451-82; ThermoFisher Scientific), anti-mouse CD4 PE (RRID:AB_2621736, 50-0041; Cytek Biosciences, Fremont, CA, USA), and anti-mouse CD25 APC (RRID:AB_312861, 102012; BioLegend) for 30 min at 4 °C. Cells were subsequently washed twice with the FCM buffer, stained with 7-aminoactinomycin D (BioLegend), and analysed on an Attune NxT Flow Cytometer (ThermoFisher Scientific). FCM data were analysed using FlowJo software (Becton, Dickinson and Company, Ashland, OR, USA). Tumour growth data were statistically evaluated using the Wilcoxon rank sum test in the GraphPad Prism software (GraphPad Software, Inc., La Jolla, CA, USA).

Transwell migration assay

Transwell migration assays were performed as previously described, with some modifications.[30,31] Briefly, transwells with 8-μm pore size filters (Corning Inc., Corning, NY, USA) were inserted into 24-well plates. Conditioned medium of RKO cells or RPMI 1640 medium containing 10 ng/ml of recombinant human MDK (R&D Systems, Minneapolis, MS, USA) (500 μL) was added to the lower chamber, while a 200-μL cell suspension (1×10^5 cells) of MT-2 cells in serum-free RPMI 1640 medium was added to the upper chamber. The plates were incubated at 37 °C in a 5% CO_2 atmosphere for 24 h. Cells in the lower chamber were then stained with 0.1% crystal violet solution (Sigma–Aldrich) and counted. Cells were lysed in the Laemmli sample buffer and subjected to Western blotting.

Analytical methods

Data pre-processing

We downloaded raw-count matrix data of 3′-end scRNA-seq data (10× Genomics) on 63689 cells from 23 primary CRC and 10 matched normal samples from 23 CRC patients from GSE132465.[19] Data were processed using the python package, Scanpy (v 1.8). Briefly, as described in the tutorial (https://scanpy.readthedocs.io/en/stable/tutorials.html), to identify highly variable genes, where genes detected in less than 3 of total cells and cells with <200 expressed genes were removed and selected according to the following criteria: cells with <2500 genes and <5% mitochondrial gene expression in unique molecular identifier (UMI) counts, the count matrix being normalised to 10,000 per cell by the total number of UMIs per cell and log-transformed by adding one and standardised for each gene. Highly variable genes were selected based on specific thresholds for mean expression and dispersion using *scanpy.pp.highly_variable_genes* (min_mean = 0.08, max_mean = 4, min_disp = 0.7).

Integrative analysis and colocalisation analysis using DeepCOLOR

Colocalisation analysis was performed using the package, DeepCOLOR, a computational framework based on a deep generative model which integrates spatial and single-cell transcriptome data to recover co-localisation relationships between single cells.[23] Here, we briefly introduce DeepCOLOR; details of the algorithms and

benchmarking are described by Kojima et al., (2022). First, DeepCOLOR derives latent cell states from single-cell transcriptomes based on a variational auto encoder,[32] which summarises high dimensional expression profiles into low dimensional cell states via an encoder and reconstructs the expression profiles of these cell states using a decoder. Next, it assumes a neural network that transforms the cell states into spatial distributions on the tissues observed by the spatial transcriptome and optimises that neural network to maximise the generative probability of observed spatial gene expression patterns via multiplication of the spatial distribution with reconstructed expression profiles of various cell states. Based on the optimised spatial distribution of single cells, the co-localisation network between single cells (which helps identify cell populations based on co-localisation), can be reconstructed and cell–cell interactions of co-localised cells, which occur via Ligand–Receptor interactions, can be estimated.

Following scRNA-seq pre-processing, we excluded genes with total counts <10 and aligned genes for both scRNA-seq and spatial transcriptomics data using selected highly variable genes. We combined the estimated spatial distribution of single cells with their expression profiles using *deepcolor.estimate_spatial_distribution* with specified optional parameters (first_epoch = 500 and second_epoch = 500). We then conducted and visualised uniform manifold approximation and projection (UMAP) embeddings of the latent states of single cells. For the subset analysis, we reconstructed UMAP in the extracted cell population. Spatial gene expression was examined with the imputed expression estimated after integration using *deepcolor.calculate_imputed_spatial_expression*. To identify cell populations associated using specific pathological tissue annotations, we aggregated the spatial assignment of each single cell on spatial spots, annotated as normal, adenoma, or carcinoma using the pathological image. The proportion of these aggregated assignments to the total spatial assignment of each cell was calculated, and the most appropriate cell population with the top-10% for each annotation across six cell types (epithelial, T, B, stromal, and mast cells; monocytes) was extracted. The cell proportions in the spatial distribution of cell types and cell subtypes were estimated using *deepcolor.calculate_clusterwise_distribution*.

In the colocalisation analysis, cell pairs with high colocalisation scores were clustered using *deepcolor.analyze_pair_cluster* with a specified optional parameter (max_pair_num = 30000). The clusters of colocalised single-cell pairs were based on the scores observed between two cells that were uniformly mapped to each spatial spot. The spatial distribution of colocalised cell clusters was estimated using *deepcolor.calculate_clusterwise_distribution*.

Ligand activity analysis using DeepCOLOR

We identified candidates for ligand–receptor communication between colocalised single cells using *deepcolor.calculate_proximal_cell_communications* with specified optional parameters (ntop_genes = 1000, cell-type_sample_num = 500). In this implementation, the strength of the ligand-receptor communication is quantified by the number of colocalised cell pairs where sender cells exhibit the top-10% expression of ligands and receiver cells exhibit the top-10% ligand activity. The ligand activity scores are calculated by *scanpy.tl.score_genes* for the top-1% target genes derived from a ligand-target matrix described as follows. We utilised ligand–receptor pair data from diverse sources[33–43] to construct a weighted network using the *construct_weighted_networks* and *apply_hub_corrections* functions from the 'nichenetr' package.[37] During this process, the signalling network and the genetic regulation network were integrated, with weight adjustments performed for each edge. The *construct_ligand_target_matrix* function was then employed to generate a ligand–target matrix. This was achieved using the constructed weighted network to estimate the regulatory potential scores for each ligand–target pair. The computations were performed using the Personalized PageRank (PPR) algorithm.[44]

Enrichment analysis

Cluster-based detection of Differentially Expressed Genes (DEGs) was performed using the Wilcoxon rank-sum test and Benjamini–Hochberg method[45] to correct for multiple comparisons (*scanpy.tl_rank_genes_groups*). DEGs with adjusted $p < 0.05$ and log 2 fold changes >0.5 were included. Based on DEGs, GO and Reactome pathway analyses were performed using *scapy.queries.enrich*.

Public datasets

TCGA CRC mRNA expression data (version 2017-09-08) were downloaded from UCSC XENA (http://xena.ucsc.edu/). We obtained gene-level transcription estimates as log 2 (x + 1) transformed RSEM normalised counts, and clinical information for CRC patients. The association between survival and gene expression levels was analysed using the R (4.2.0) package, survival (3.5.5). Overall survival (OS) was estimated using the Kaplan–Meier method, and the survival curves were compared using the log-rank test. Univariate and multivariate analyses were performed using the Cox proportional hazards model to identify independent variables predictive of OS; $p < 0.05$ was considered statistically significant. A CRC single T cell sequencing dataset was downloaded from GSE108989. The data processing methods were described in the original article.[46] Mutation annotation data for 2844 CRC patients were obtained from the Catalogue of Somatic Mutations in Cancer (COSMIC) database (https://cancer.sanger.ac.uk/cosmic).

Ethics

All patients were treated according to the Japanese Society of Cancer of the Colon and Rectum Guidelines for the Treatment of Colorectal Cancer. The study was approved by the Kyushu University Institutional Review Board (approval #2021-337 and #2022-131). All data were de-identified prior to use in the study. All investigations carried out in this study were performed in accordance with the tenets of the Declaration of Helsinki.

Statistics

The statistical analyses were performed using R software v4.2.0 and Python v3.9.16. Associations between variables were analysed using Welch's t-test, the Wilcoxon rank sum test, and one-way ANOVA. Overall survival (OS) curves were plotted according to the Kaplan–Meier method and compared using the log-rank test. Patient data in survival analyses were divided into with high and low mRNA expression by median expression levels. Univariate and multivariate analyses were carried out using the Cox proportional hazards model to identify independent variables predictive of OS. The Schoenfeld residuals diagram was performed to verify the proportional hazards assumption. A two-sided p value < 0.05 was deemed statistically significant.

Role of funders

The funders of the study had no role in the study design, data collection, data analysis, data interpretation, writing the paper, and in the decision to submit the paper for publication.

Results

Single-cell and spatial transcriptome profiling in CRC

We generated ST-seq data for five cases of carcinoma in adenomatous polyps, and for one case of advanced CRC to unravel TME construction associated with multistep carcinogenesis of CRC (Supplementary Data 1). ST-seq and public scRNA-seq data for 23 Asian patients from GSE132465 (33 samples: 23 cancer cases and 10 normal tissues)[19] were integrated using DeepCOLOR (Fig. 1a). ST-seq cases were divided into normal, adenoma, and carcinoma regions by mucosal layer for early CRC, and into normal and carcinoma regions for advanced CRC (Fig. 1b; Supplementary Figure S1); scRNA-seq contained 63,689 cells; cell annotation was performed as in the dataset, classified by 6 cell types and 30 cell subtypes (Fig. 1c).

Following integration using DeepCOLOR, the abundance at the single-cell level in the spatial distribution of each pathological diagnosis was compared for each cell type and subtype (Fig. 1d and Supplementary Figure S2a and b). Normal epithelial cell types were classified as normal, and tumour epithelial cells were specifically classified as adenoma or carcinoma, confirming successful integration. Next, to describe the tissue origin, we calculated the proportion of the aggregated assignments based on spatial pathological diagnosis and defined the top-10% of each of the six cell types in normal, adenoma, and carcinoma regions as cells with distinctive tissue origins (Fig. 1e; Supplementary Figure S2c and d). We then identified 17,442 cells as these specific cells and confirmed that the spatial distribution of epithelial cells in each specific tissue origin was in close agreement with the pathological diagnosis (Fig. 1f; Supplementary Figures S2e and S3).

Regulatory T cells were enriched in carcinoma in adenomatous polyps

In order to clarify the characteristics of early-stage CRC, we extracted epithelial cells and conducted gene ontology (GO) analysis for cancer and adenoma epithelial cells (Fig. 2a, Supplementary Data 2). Cancer epithelial cells were enriched in processes associated with cell proliferation and invasive potential, which result was consistent with that of pathological diagnosis (Fig. 2b). Additionally, immune-related pathways were enriched in the Reactome pathway analysis (Supplementary Figure S4a). Next, we extracted and analysed T cells in the same manner (Fig. 2c and d). The pathway related to the activity of Tregs was the most enriched, indicating that Tregs may affect immune tolerance activities during carcinogenesis. We performed GO and pathway analyses for all other cell types. GO analysis showed enrichment of processes involved in cancer-induced angiogenesis in fibroblasts (Supplementary Figure S4b).

We determined the proportion of cell subtypes identified by integrative analysis using DeepCOLOR in pathological diagnosis on ST-seq to assess the infiltration of Tregs in early-stage CRC (Fig. 2e). Consistent with the pathological diagnosis, the number of tumour epithelial cells increased with tumour progression. The proportion of T cell subtypes, especially CD4+ T cells and Tregs, in cancer tissues was higher than that in normal tissues. Importantly, the proportion of CD4+ T cells was not significantly different between adenoma and normal tissue, whereas that of Tregs was significantly higher in adenoma and carcinoma tissues (Fig. 2f and g). Tregs play a strong immunosuppressive role in the TME, inhibiting anti-tumour immunity and contributing to tumour progression.[47] Furthermore, tissue localisation of Tregs is associated with poor prognosis in many types of cancer, including head and neck, liver, gastrointestinal tract, pancreatic, breast, and ovarian cancer.[48–58] In CRC and adenomas, scRNA-seq trajectory analysis showed an increase in the proportion of Tregs in late-stage adenoma and cancer,[22] suggesting that the increase in Treg proportion in adenoma may be associated with immune tolerance, starting from the precancerous stage.

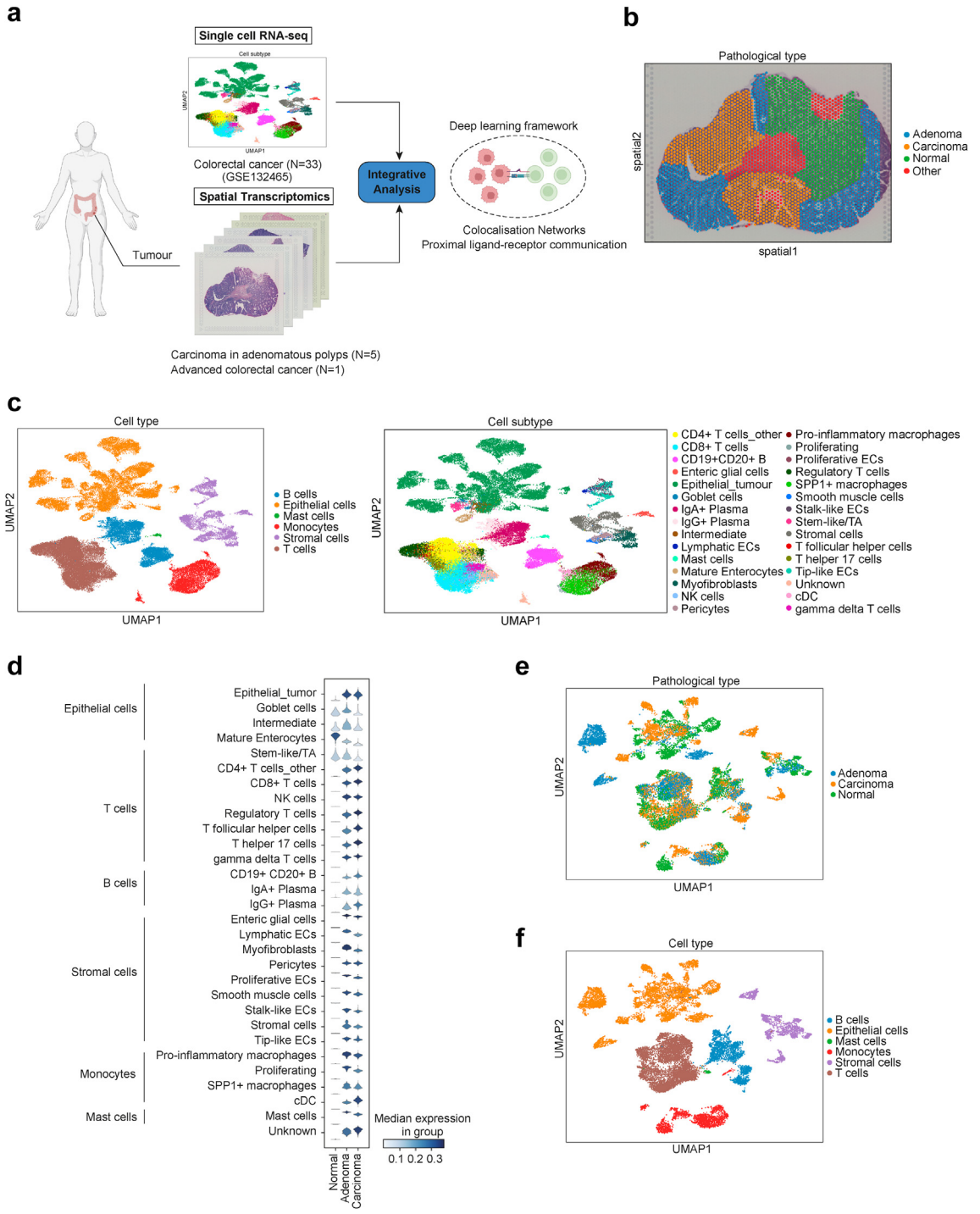

***Fig. 1:* Single-cell decomposition of scRNA-seq colorectal cancer (CRC) dataset and spatial mapping of single cells.** (a) Schematic of library collection and integrative analysis of single-cell and spatial transcriptomics of CRC. (b) Spatial visualisation of clustering on the CRC sample slide. (c) Uniform manifold approximation and projection (UMAP) of all colorectal cancer cell types and subtypes. (d) Stacked violin plots of spatial assignment to each pathological diagnosis for 30 cell subtypes. (e and f) UMAP of specific tissue origins (e) and cell types (f) after the definition of cell origin filtering of the top-10% based on each pathological diagnosis.

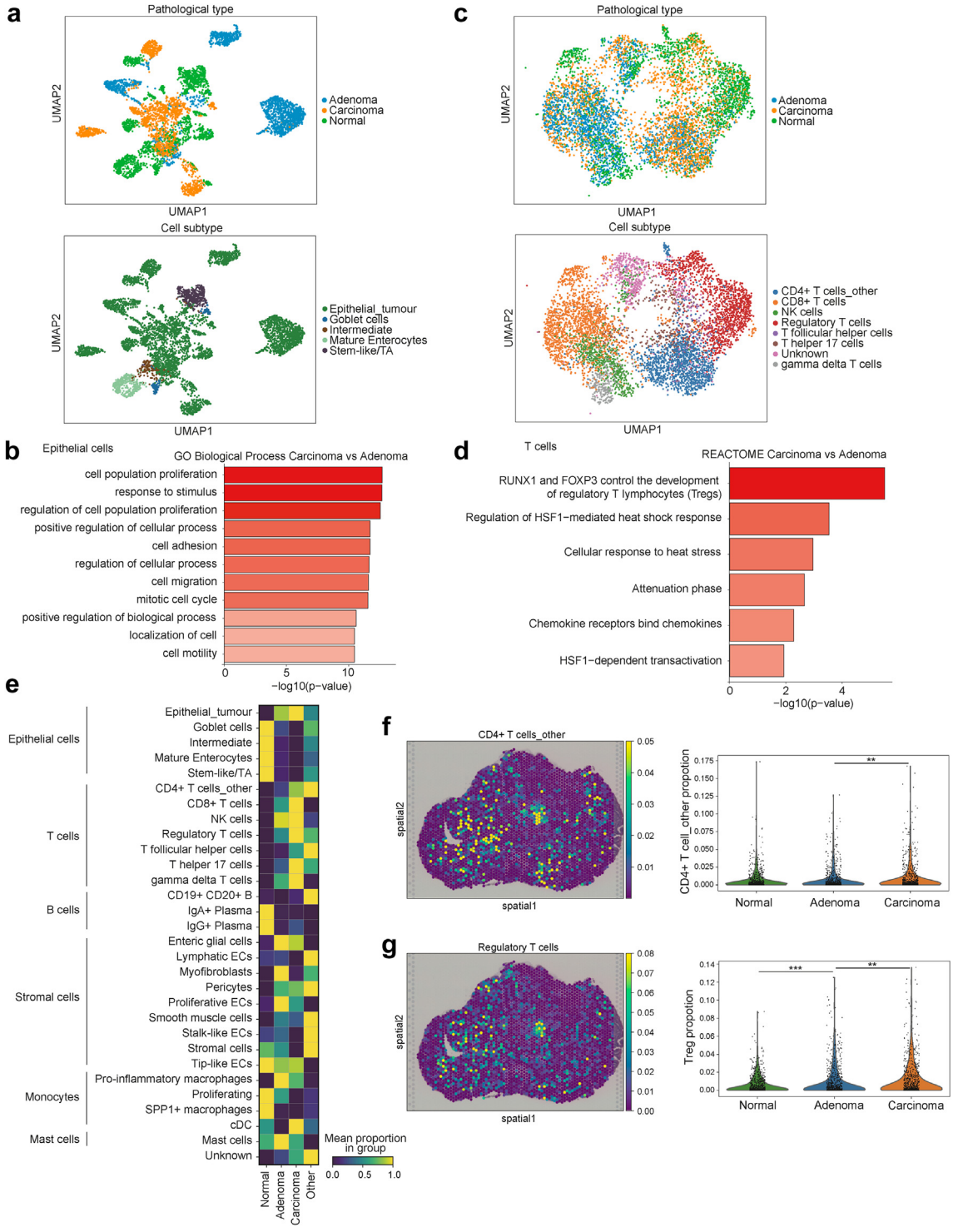

***Fig. 2:* Characteristics of epithelial and T cells and cell proportions in spatial distribution**. (a) Uniform manifold approximation and projection (UMAP) of epithelial cells in spatial distribution after filtering. (b) Gene ontology (GO) analysis of biological process comparing carcinoma and adenoma epithelial cells. (c) UMAP of T cells in spatial distribution after filtering. (d) Reactome pathway analysis comparing carcinoma and adenoma T cells. (e) Heatmap of the mean proportion values per spatial pathological diagnosis of each cell subtype. (f and g) Spatial distribution following the reconstruction of spatial gene expression patterns and violin plots of proportions based on pathological diagnosis, in CD4+ T cells_other (f) and regulatory T cells (g); **, $p < 0.01$; ***, $p < 0.001$; p values were determined using Welch's t-test.

Adenoma epithelial cells colocalised with tregs and interacted via MDK

To explore Treg-mediated immune tolerance in adenoma, we examined epithelial cells that colocalised with Tregs in adenomas. DeepCOLOR derives the colocalisation profile for two cells from the overlapping spatial distribution of single cells, and clusters adjacent single-cell pairs to classify the populations. Of the 5168 cells defined as adenoma-specific cells, 1702 epithelial cells and Tregs were co-localised (Fig. 3a and b; Supplementary Figure S5a). Epithelial adenoma cells that were colocalised with Tregs were particularly abundant at the adenoma–carcinoma interface and in adenoma regions in the vicinity of carcinoma. Tregs were also present in the stroma of colocalising epithelial cells (Fig. 3c).

We predicted ligand-mediated intercellular communication using DeepCOLOR between colocalised cells by combining data for colocalisation scores, gene expression in single cells, and ligand–receptor relationships and their downstream signalling information. Cell–cell interaction inference highlighted MDK as a molecule that enables communication between adenoma epithelial cells and Tregs (Fig. 3d). MDK is a secreted protein, the expression of which is highly increased in various cancers in addition to being associated with tumour cell proliferation, transformation, epithelial–mesenchymal transition, angiogenesis, mitogenesis, anti-apoptosis, and chemotherapy resistance.[59] We assessed MDK expression in carcinoma and adenoma and found that most epithelial cells in colocalisation clusters expressed MDK (Fig. 3e and f). Furthermore, we analysed differentially expressed ligand genes between adenoma epithelial cells colocalised with Tregs or other adenoma epithelial cells and identified 313 genes. MDK was a significantly highly expressed ligand gene in colocalised cells (Fig. 3g and h; Supplementary Data 3). GO analysis revealed that proliferative capacity-related processes were enriched in colocalised adenoma epithelial cells than in other adenoma epithelial cells (Fig. 3i). Moreover, we performed in vivo validation to confirm Mdk-mediated tumour growth and Treg induction as previously reported in melanoma.[60] Using the mouse colon cancer cell line, MC38, we confirmed that the proportion of Tregs in tumour tissues from cells overexpressing Mdk was significantly increased and that the proliferative potential of these cells was enhanced in an immune-dependent manner (Supplementary Figure S6). These results suggested that MDK was associated with immune tolerance of Tregs to tumour growth in CRC.

By contrast, Tregs that were colocalised with adenoma epithelial cells were found to act on those cells via T cell immunoreceptors with Ig and ITIM domains (TIGIT; Supplementary Figure S5b). TIGIT is an inhibitory immune checkpoint protein that is expressed on activated CD8+ T cells, CD4+ T cells, Tregs, and NK cells, and inhibits immune cell-mediated antitumour responses.[61–63] TIGIT was highly expressed in most Tregs colocalised with adenoma epithelial cells, indicating immune tolerance by Tregs (Supplementary Figure S5c). With respect to spatial distribution, TIGIT was highly expressed in the stroma of carcinoma and adenoma regions (Supplementary Figure S5d). Furthermore, several ligands from Treg-colocalised adenoma epithelial cells interacted with monocytes and stromal cells. Specifically, we found the involvement of LCN2, an anti-inflammatory regulator that acts on SPP1+ macrophages,[64] EDN1, which promotes fibroblast activation, proliferation, and differentiation into myofibroblasts,[65] and MMP7, which acts on fibroblasts in CRC and promotes angiogenesis (Fig. 3d).[66]

Thus, our results suggested that Treg-colocalised adenoma epithelial cells with high MDK expression not only interact with Tregs to induce immune tolerance and promote cell proliferation but also act on monocytes and stromal cells, thereby initiating TME formation in pathological adenoma.

Identification of networks of tumour-promoting and immunosuppressive environments driven by MDK

We analysed the colocalisation between carcinoma epithelial cells and Tregs. Among 6871 cells defined as having a carcinoma origin, we identified 2016 cells that colocalised with Tregs; of these 2016 cells, 1607 were epithelial cells (Fig. 4a; Supplementary Figure S7a and b). Pathological diagnosis indicated that epithelial carcinoma cells colocalised with Tregs were distributed throughout the cancerous region. Colocalised Tregs were also widely distributed in the stromal regions of the carcinoma (Fig. 4b; Supplementary Figure S7c). The colocalised cell population was subclustered into seven clusters based on single-cell pair colocalisation scores (Fig. 4c). Comparison of MDK expression in colocalisation clusters of epithelial cells showed that 1401 cells were present in clusters 0, 1, 2, and 3 with high MDK expression, and that these cells accounted for 87.2% of all colocalised epithelial carcinoma cells, indicating that most epithelial carcinoma cells which were colocalised with Tregs showed high MDK expression (Fig. 4d).

Next, we identified colocalisation clusters between epithelial carcinoma cells-colocalised Tregs and monocytes and stromal cells (Supplementary Figure 7d and 7e). When cell–cell interactions were examined for colocalised clusters, ligands similar to those found in adenoma were detected, with the same TME being formed following carcinogenesis (Fig. 4e and f). In cell–cell interactions between colocalised epithelial carcinoma cells and Tregs, we detected CXCL14, CCL2, and CCL4, which are involved in activating Tregs as well as in suppressing cytotoxic T cells.[67–70] Following carcinogenesis, colocalised epithelial cells with high MDK expression also acted on Tregs with other cytokines involved in immune tolerance (Supplementary

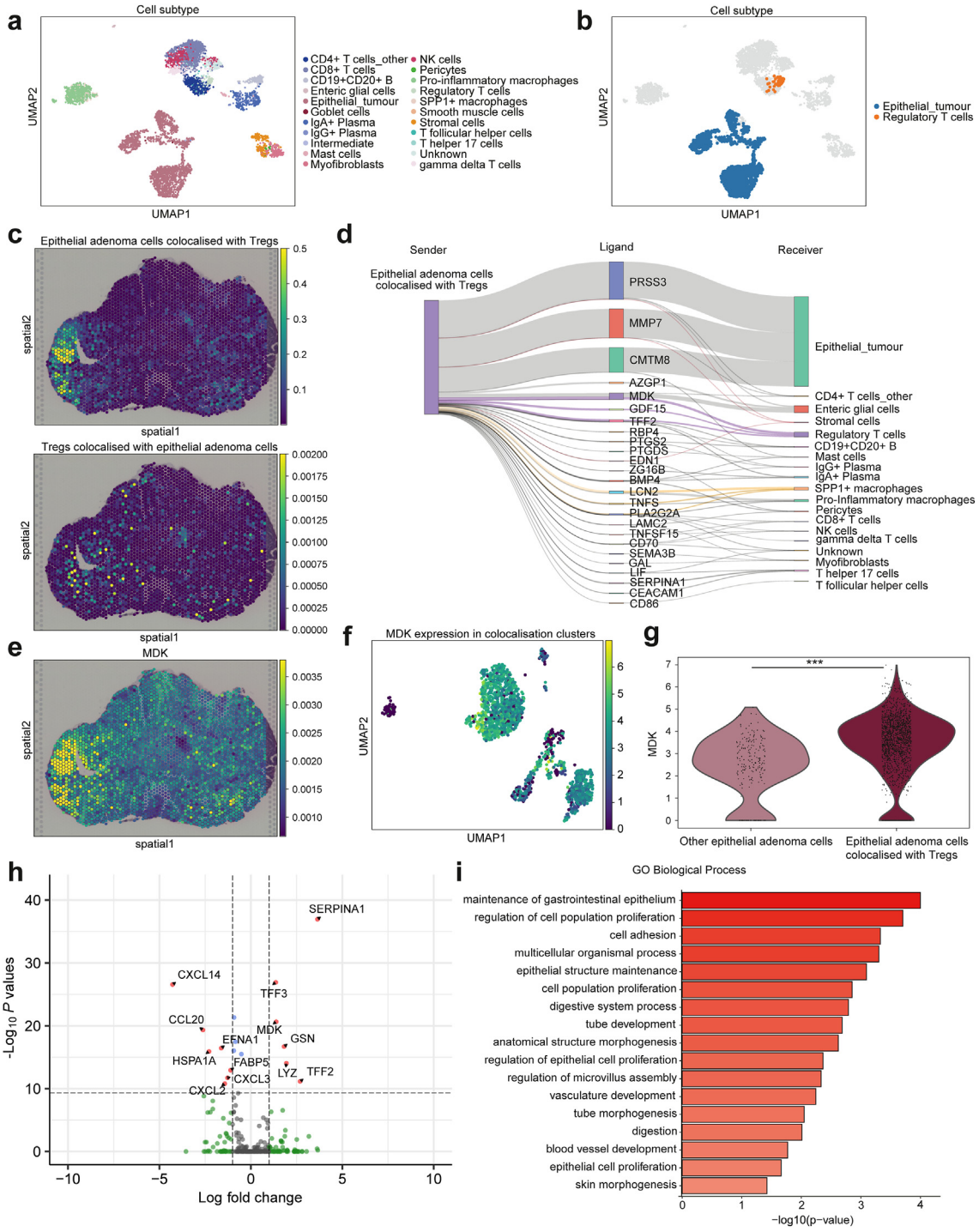

***Fig. 3:* Colocalisation analysis and cell–cell interaction of adenoma epithelial cells and regulatory T cells.** (a) Uniform manifold approximation and projection (UMAP) of cell subtypes in adenoma cluster. (b) Colocalisation clusters between adenoma epithelial cells and regulatory T cells (Tregs) in UMAP representation across all adenoma cells. (c) Spatial distribution of colocalised adenoma epithelial cells (upper) and Tregs (lower). (d) Ligand activity between colocalised single cells from epithelial adenoma cells colocalised with Tregs to other cells. The widths of the lines correspond to the ligand activity scores. (e) Imputed MDK expression in spatial distribution. (f) MDK normalised expression in colocalised cell populations in UMAP representation. (g) Violin plot representing MDK normalised expression in colocalised adenoma epithelial cells and other epithelial adenoma cells. ***$p < 0.001$. p values were determined using the Wilcoxon rank-sum test and Benjamini–Hochberg method. (h) Volcano plot representing the differentially expressed ligand genes between colocalised adenoma epithelial cells and other adenoma epithelial cells. p values were determined using the Wilcoxon rank-sum test and Benjamini–Hochberg method. (i) Gene ontology (GO) analysis of biological process comparing colocalised adenoma epithelial cells and other adenoma epithelial cells.

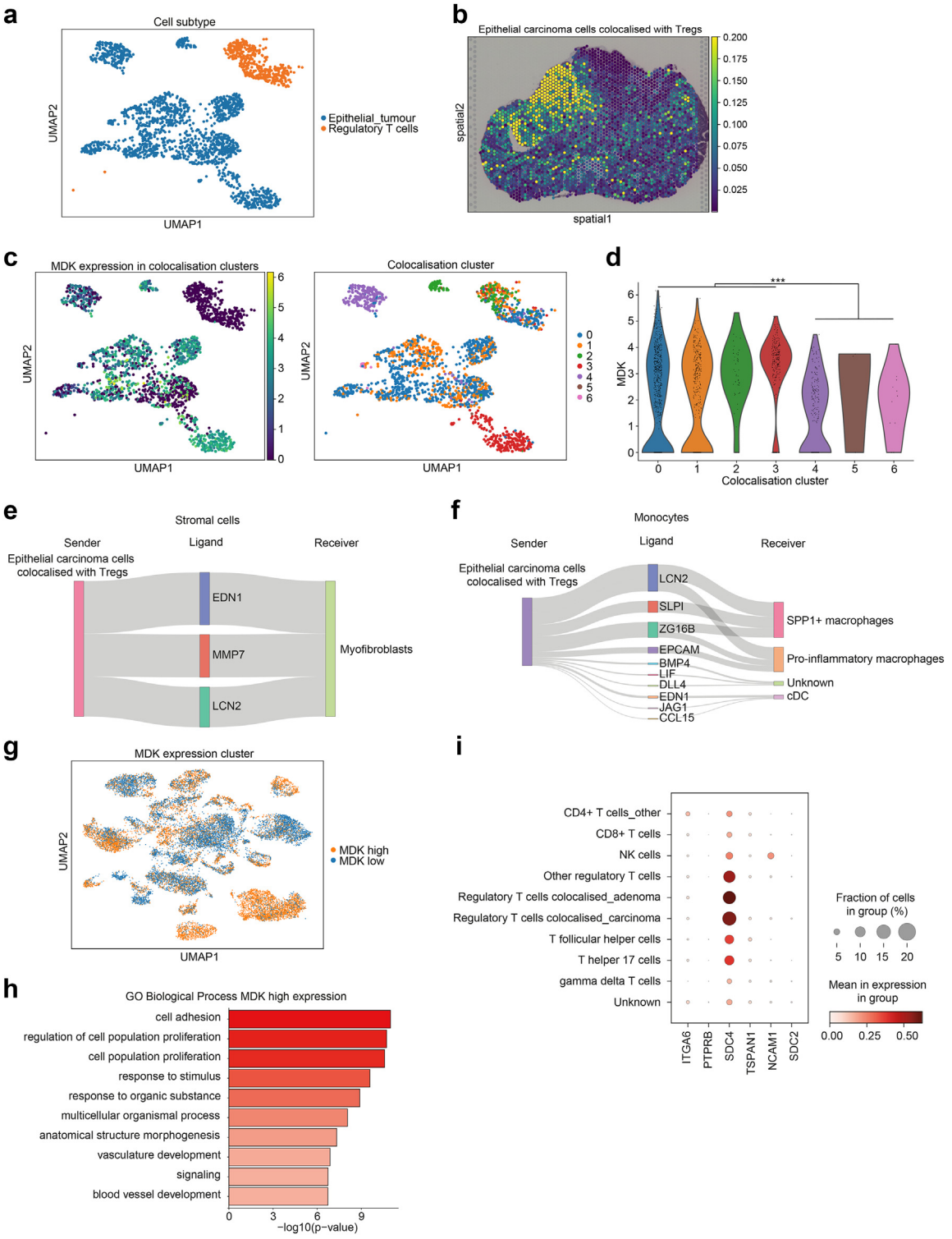

***Fig. 4:* Colocalisation analysis in carcinoma epithelial cells and cellular distribution of ligand-receptor genes in single cells.** (a) Colocalisation clusters between carcinoma epithelial cells and regulatory T cells (Tregs) in uniform manifold approximation and projection (UMAP) representation. (b) Spatial distribution of colocalised adenoma epithelial cells with Tregs. (c) MDK normalised expression and colocalisation cluster distribution in colocalised cell populations in UMAP representation. (d) Violin plot of MDK normalised expression levels by colocalisation clusters. ***$p < 0.001$. p values were determined using the Wilcoxon rank-sum test and Benjamini–Hochberg method. (e and f) Ligand activity

Figure S7f). By contrast, Tregs acted on epithelial carcinoma cells via TIGIT, a finding similar to that seen in adenomas, pointing to a Treg-mediated immune tolerance environment (Supplementary Figure S7g and h).

We then examined MDK and TIGIT expression in scRNA-seq data for 63689 cells across all cell types. MDK was most highly expressed in tumour epithelial cells, while TIGIT was most highly expressed in T cells, especially Tregs (Supplementary Figure 8a–c). Both genes were also highly expressed in colocalised tumour epithelial cells and Tregs in adenoma and carcinoma. GO analysis of epithelial cells highly expressing MDK revealed an enrichment of cell proliferation-related processes, a result that was similar to that of our colocalisation analysis (Fig. 4g and h, Supplementary Figure S8d). Furthermore, pathway analysis of T cells with high TIGIT expression showed that the pathway related to Tregs was the most enriched, confirming that TIGIT functions as an inhibitory immune checkpoint (Supplementary Figure S8e–g). We confirmed that the MDK-mediated colocalisation was consistent with scRNA-seq data for CRC.

To identify MDK receptors, we examined MDK receptor genes expressed on Tregs using ligand–receptor pair data. The distribution of the expression levels of six identified candidate genes, *ITGA6, PTPRB, SDC4, TSPAN1, NCAM1*, and *SDC2*, in T cells, revealed that *SDC4* was the most highly expressed gene in Tregs, especially in those colocalised with epithelial tumour cells (Fig. 4i; Supplementary Figure S9a and b). Additionally, we analysed the expression of MDK receptor genes on Tregs using public CRC single T cell sequencing data from GSE108989 (12 CRC cases).[46] The proportion of CD4+ CD25 high T cells, Tregs, in cancer tissue was higher than in normal tissues (Supplementary Figure S10a). We found that among the six MDK receptor candidate genes, only SDC4 was highly expressed in tumour-derived T cells, particularly in Tregs (Supplementary Figure S10b–e). These findings suggested that SDC4 may act as a receptor expressed on Tregs in MDK-mediated immune tolerance in CRC.

Reproducibility of MDK-mediated colocalisation network with multiple CRC cases

We compared the results of these integrated analyses with other ST-seq data. We integrated ST-seq and scRNA-seq data and examined colocalised-cell distribution between epithelial cells and Tregs identified in the previous analyses (Supplementary Figure S11a). In all cases of carcinoma in adenoma, epithelial tumour cells colocalised with Tregs were found at the carcinoma–adenoma interface as well as in the proximity of the cancer in adenomas (Fig. 5a; Supplementary Figure S11b). Identified adenoma and carcinoma epithelial cell clusters showed a distribution pattern that was almost the same as that detected via pathological diagnosis, confirming that other forms of integrated analysis could successfully annotate cell groups via deep learning (Supplementary Figure S1b). Additionally, the ratio of Tregs colocalised with epithelial tumour cells was high around the carcinoma–adenoma interface (Fig. 5a; Supplementary Figure S11b).

MDK-mediated formation of TME is present in CRC cases

Next, we performed immunohistochemistry and immunofluorescence staining for MDK, FOXP3, and SDC4 in other CRC cases (Supplementary Data 4). MDK and SDC4 were found to be highly and colocalisedly expressed in epithelial tumour cells and stroma at the adenoma–carcinoma interface and in the adenoma region near carcinoma (Fig. 5b and c). FOXP3 was also expressed in the same stromal area, while immunofluorescence staining indicated that SDC4 was expressed in Tregs at the adenoma–carcinoma interface and in the adenoma region near carcinoma (Fig. 5b and d). In advanced carcinomas, the same results as that observed for carcinoma in adenomatous polyps were observed in the invasive front (Supplementary Figure S12). Finally, we confirmed the spatial distribution of MDK, TIGIT, and SDC4 in all other cases (Supplementary Figure S13). These results suggested that MDK-mediated formation of TME was present in early and advanced CRC cases.

MDK-SDC4 interaction in CRC cells promotes the migration of Treg-like cells

We assumed that the MDK signalling pathway in the interaction of MDK and SDC4 ligand-receptor communication played a significant role in inducing Tregs in CRC. To validate our hypothesis, we performed a transwell migration assay using human colorectal cancer RKO cells with MDK knockdown and human regulatory T cell-like MT-2 cells with SDC4 knockdown.[27] Significant downregulation of the protein levels of MDK-knockdown RKO cells and SDC4-knockdown MT-2 cells was observed (Fig. 6a and b). The transwell migration assay showed that, compared with the control,

initiating from epithelial carcinoma cells colocalised with regulatory T cells (Tregs) to colocalised stromal cells (e) and monocyte cells (f) The widths of the lines correspond to the ligand activity scores in e and f. (g) UMAP distribution in comparison of epithelial cells with high and low MDK expression divided by median MDK expression levels. (h) comparative Gene ontology (GO) analysis of biological processes associated with high and low MDK expression in epithelial cells. (i) Dot plot of the expression and proportion of MDK receptor genes per cell subtype in T cells; the circle size represents the cell proportion.

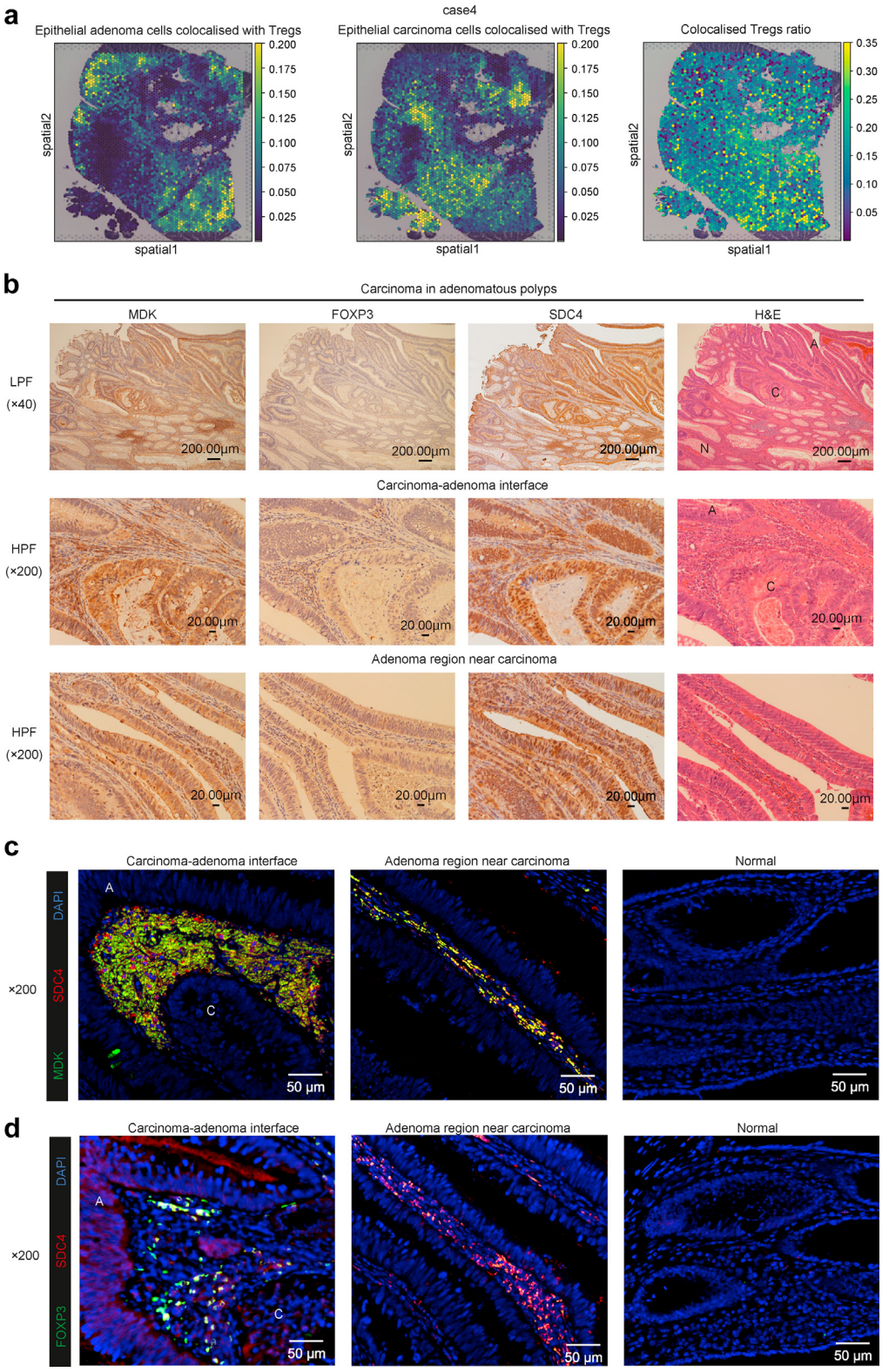

Fig. 5: **Distribution of colocalised cells between epithelial cells and regulatory T cells and MDK, FOXP3, and SDC4 expression in carcinoma in adenomatous polyps**. (a) Spatial distribution of epithelial cells colocalised with regulatory T cells (Tregs) and colocalised Tregs ratio in other

the knockdown of MDK in RKO cells and SDC4 in MT-2 cells significantly decreased the migration of MT-2 cells (Fig. 6c). Interestingly, the addition of MDK protein to conditioned medium of MDK-knockdown RKO cells showed a significant effect on MT-2 migration, while its addition to serum-free medium showed no significant difference (Fig. 6d). These results suggest that other secreted molecules, not MDK, could act as chemotactic agents for Tregs, and SDC4 interaction could interact with MDK secreted in CRC and promote the motility of Treg migration, resulting in immunosuppressive environments.

High MDK and SDC4 expression levels predict poor prognosis in patients with CRC

MDK, which is highly expressed in various tumours, shows potential as a potential diagnostic and prognostic cancer biomarker.[59,71,72] Reportedly, serum MDK acts as a prognostic biomarker in CRC.[73] We investigated the association between *MDK* expression and prognosis using RT-quantitative PCR (qPCR) in paired normal and cancer tissues from our CRC cohort data. *MDK* expression in cancer tissues was significantly higher than that in normal tissues. In addition, the TN ratio at each T stage increased as the T stage progressed, and was higher not only in advanced cancer but also in the early stages of Tis and T1 (Fig. 7a and b). This suggested that *MDK* expression in early-stage CRC tissues was higher than that in normal tissues. Our cohort data and The Cancer Genomics Atlas (TCGA) data showed that groups with high *MDK* and *SDC4* expression received poor prognoses (Fig. 7c). Notably, the group showing high expression levels of both *MDK* and *SDC4* received the poorest prognoses (Fig. 7d). Furthermore, *MDK* expression in cancer tissues showed potential as an independent prognostic factor in multivariate analysis (Table 1, Supplementary Figure S14a). The detection of only a few MDK and SDC4 mutations indicated that the inhibition of their expression in the MDK/SDC4 pathways may be a potential therapeutic target (Supplementary Figure S14b). Considered together, these findings suggested that MDK and SDC4 may act as mediators that are essential for immunotherapeutic targeting in CRC, given their links with poor prognoses.

Discussion

We constructed a single-cell transcriptome atlas of cell populations in CRC using publicly available scRNA-seq data and performed an integrated analysis using DeepCOLOR, a deep-learning computational framework, with ST-seq data for early and advanced CRC.[19,23] This integrated analysis helped overcome the limitations of sample collection and allowed for more complex transcriptome analyses than would be feasible with histopathological diagnosis. We utilised this deep learning framework to identify colocalised cells and gain insights into the TME by examining cell–cell interactions.

Interaction between tumour cells and immune cells affects cancer development. Thus, regulation of such interactions plays an important role in immunosuppression in cancer.[74] Tregs in the TME of various cancer types are believed to be involved in immune tolerance.[47] Herein, we found that Tregs contribute to immune tolerance in the adenoma–carcinoma sequence during the early stages of cancer. In CRC, MDK induces the colocalisation of Tregs in the TME (Fig. 7e). Such colocalisation was prominent at the adenoma–carcinoma interface of adenomas. This is the first study indicating MDK-mediated induction of immune tolerance in adenomas during the early stages of cancer. MDK is a secreted protein that drives immune cell chemotaxis.[59] TAM- and T cell-mediated immune tolerance associated with elevated MDK in epithelial cells has been reported in melanoma and gallbladder cancer.[60,71] Similarly, MDK-mediated immune tolerance is believed to manifest during early-stage CRC. Thus, MDK represents an important target in immunotherapy. Although MDK is highly expressed in various cancers, it is also involved in normal-cell growth and division as well as in the regulation of blood vessel formation and function.[75] Therefore, in order to minimise off-target effects of direct MDK inhibition, it is necessary to inhibit the pathway associated with tumour-specific MDK signaling, via the development of selective inhibitors of the MDK receptor in cancer tissues. In this study, we identified SDC4, which encodes the MDK receptor on the Treg cell-membrane surface. SDC4 which binds MDK,[76] is closely associated with the development of osteosarcoma, breast cancer, prostate cancer, colorectal cancer, and many other cancers.[77–80] SDC4 reportedly acts as a main endogenous membrane-associated receptor, which regulates cell migration and cell adhesion in tumourigenesis and progression. Moreover, SDC4 promotes cell migration by affecting several signalling pathways, such as regulating Rac 1 GTPase activity, regulating focal adhesion kinase, protein kinase C-alpha, and the level of intracellular calcium.[81–85] We also showed that MDK-SDC4

carcinoma in adenomatous polyps, case 4. Colocalised Tregs ratio is calculated as the proportion of Tregs colocalised with epithelial tumour cells among all Tregs. (b) Immunostaining of MDK, FOXP3, and SDC4 in carcinoma in adenomatous polyps. Pathological diagnosis by H&E staining; N: normal tissue, A: adenoma tissue, C: carcinoma tissue. (c) Immunofluorescence images of MDK, SDC4, and DAPI expression in carcinoma in adenomatous polyps. (d) Immunofluorescence images of FOXP3, SDC4, and DAPI expression in carcinoma in adenomatous polyps. A: adenoma tissue; C: carcinoma tissue.

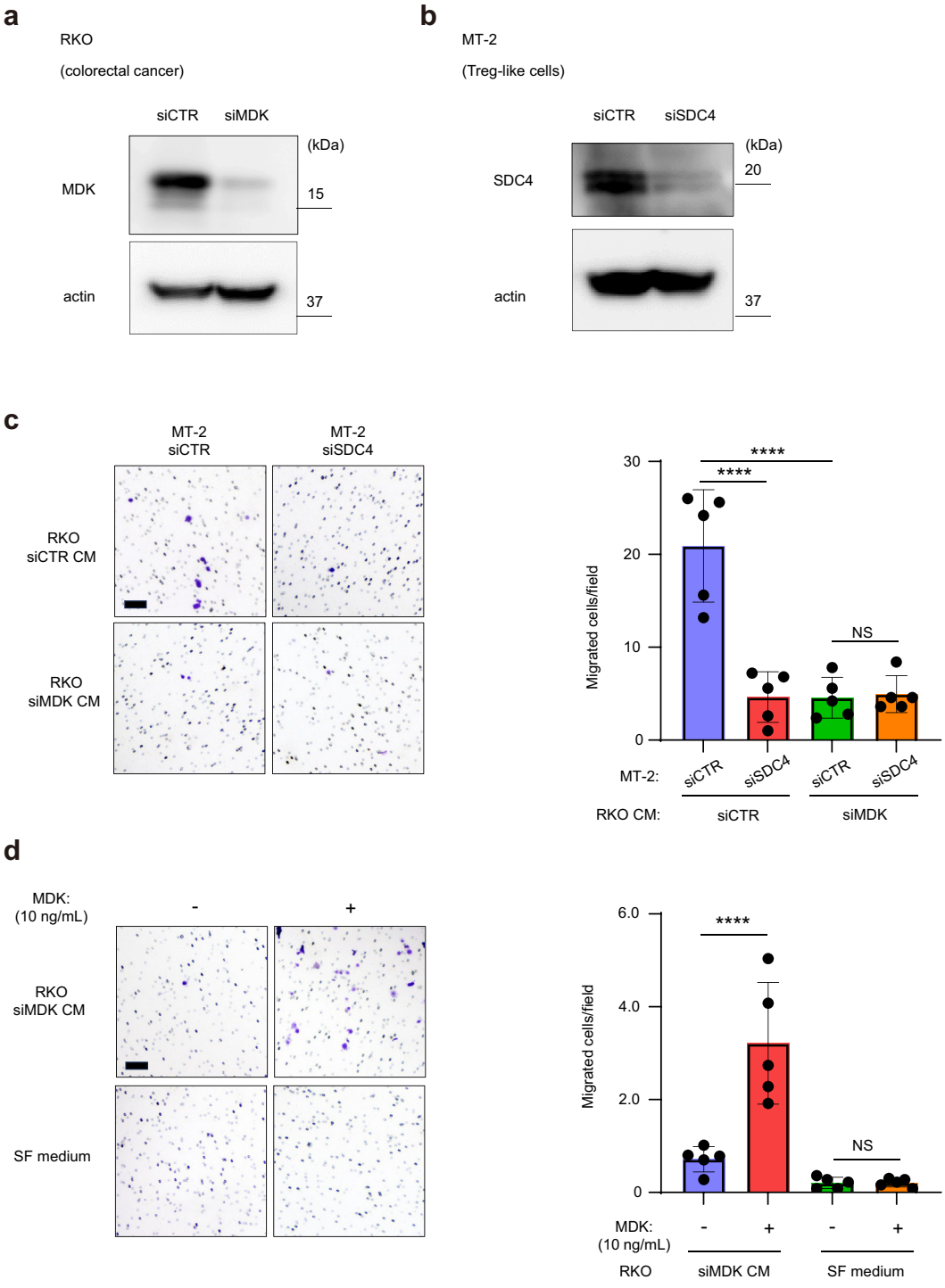

***Fig. 6:* MDK and SDC4 promote the migration of Treg-like cells in colorectal cancer (CRC) cells.** (a) Immunoblotting for MDK in control and MDK-knockdown CRC cells (RKO). (b) Immunoblotting for SDC4 in control and SDC4-knockdown Treg-like cells (MT-2). (c) Transwell migration assays of control and SDC4-knockdown MT-2 cells with conditioned medium of control and MDK-knockdown RKO cells. (d) Transwell migration assays of MT-2 cells with conditioned medium of MDK-knockdown RKO cells and serum-free medium containing 10 ng/ml of recombinant human MDK; NS, $p > 0.05$; ****, $p < 0.0001$. p values were determined using one-way ANOVA, followed by Dunnett's multiple comparisons test. Scale bar, 100 μm.

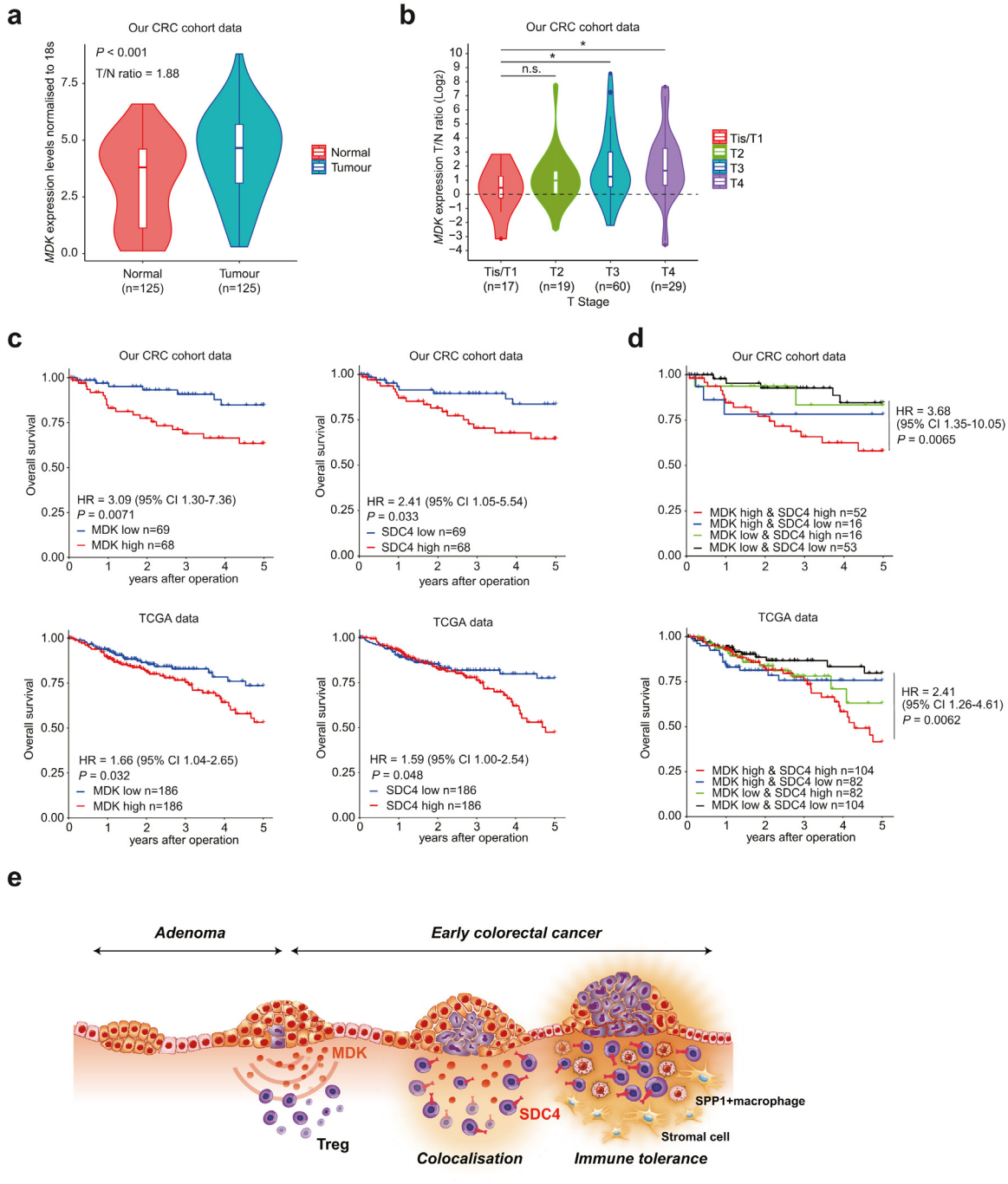

***Fig. 7*: Clinical significance of *MDK* and *SDC4* expression in human colorectal cancer (CRC).** (a) *MDK* mRNA expression in 125 CRC tissues and paired normal colon tissues in our CRC cohort dataset, assessed using RT-quantitative PCR; *p* values were determined using the Wilcoxon rank sum test. (b) Expression ratio of *MDK* in tumour and normal tissues by pathological T stage; NS, $p > 0.05$; *, $p < 0.05$. *p* values were determined using one-way ANOVA, followed by Dunnett's multiple comparisons test. (c) Overall survival rate in CRC patients according to *MDK* and *SDC4* mRNA expression in tumour tissues in our CRC cohort data (top) and The Cancer Genomics Atlas (TCGA) data (bottom). (d) Overall survival rate in CRC patients by the combination of *MDK* and *SDC4* mRNA expression in tumour tissues in our CRC cohort data (top) and TCGA data (bottom). Overall survival was estimated using the Kaplan–Meier method, and survival curves were compared using the log-rank test. CI: confidence interval; HR: hazard ratio. (e) Schematic of tumour MDK-mediated immunosuppressive environment in early CRC.

Variables	HR	Univariate (95% CI)	p value	HR	Multivariate (95% CI)	p value
Age (<65 y/≥65 y)	2.42	1.12–5.24	0.025	1.57	0.66–3.70	0.31
Gender (female/male)	1.18	0.55–2.55	0.68			
Size (≥5 cm/< 5 cm)	1.79	0.83–3.87	0.14			
Tumour location (right/left)	1.25	0.57–2.76	0.58			
Histological type (muc, por/well, mod)	7.02	2.35–20.97	<0.01	7.35	2.08–26.01	<0.01
T stage (3,4/is, 1, 2)	12.92	1.75–95.49	0.012	5.94	0.77–45.87	0.087
Lymph node metastasis (+/−)	6.85	2.36–19.91	<0.01	3.06	0.97–9.68	0.057
Distant metastasis (+/−)	15.05	4.04–56.08	<0.01	10.66	2.61–43.45	<0.01
Lymphatic invasion (+/−)	5.41	2.26–12.95	<0.01			
Venous invasion (+/−)	4.3	1.98–9.37	<0.01			
pStage (III, IV/0, I, II)	10.03	3.01–33.45	<0.01			
MDK expression (high/low)	3.09	1.30–7.36	0.011	2.73	1.04–7.13	0.041

CI, confidential interval; CRC, colorectal cancer; HR, hazard ratio; muc, mucinous adenocarcinoma; por, poorly differentiated adenocarcinoma; well, well-differentiated adenocarcinoma; mod, moderately differentiated adenocarcinoma.

Table 1: **Univariate and multivariate analysis of clinicopathological factors affecting the overall survival in patients with colorectal cancer.**

interaction in CRC cells promotes the migration of Treg-like cells. These findings show thet SDC4 could potentially be a new therapeutic candidate. Further exploration will be required to elucidate the mechanism underlying the effects exerted by SDC4 on Tregs in CRC.

Previously, we showed that multiple subclones harboring different mutations in driver genes that appear during the early stages of tumourigenesis are responsible for tumour heterogeneity.[12,13] Immune tolerance resulting from MDK secretion at the adenoma–carcinoma border may contribute to this process. Furthermore, we reported two intriguing findings regarding the regulation of MDK expression: binding of HIF-1a to hypoxia-responsive elements in the MDK promoter region, and activation by Wnt/β-catenin signaling.[86,87] The MDK promoter region harbors a binding site for TCF/LEF interacting with APC/β-catenin. The frequent occurrence of APC mutations in colorectal adenomas and carcinomas,[7] indicates that upregulation of Wnt/β-catenin signaling may be involved in increased MDK expression. Further investigation is needed to examine the association between these regulatory processes and MDK expression in CRC.

Using spatial analysis at the single-cell level, we identified MDK and noted that interaction between colocalised Tregs and tumour epithelial cells is mediated via TIGIT. These results are novel, considering the fact that mediator molecules that confer immune tolerance have not been reported in previous single-cell studies on adenoma and early CRC. TIGIT is an inhibitory receptor that directly reduces T-cell receptor signaling in T cells. TIGIT has been focused upon as a target for immune checkpoint therapy in cancer. Clinical trials of anti-TIGIT antibody in combination with anti-PD-1/PD-L1 antibodies in patients with various solid tumours have shown favorable antitumour effects.[88] MDK may be an important biomarker that predicts the therapeutic efficacy of these new immunotherapies in CRC.

A limitation that affected this study was that scRNA-seq and ST-seq were not implemented using identical samples. Therefore, all intra-adenoma cancer-specific cell populations may not have been captured. However, to overcome this issue, we performed an integrated analysis using scRNA-seq data from a large number of cases.

Finally, our clinical analysis showed that *MDK* expression was high in early CRC stages and that MDK and SDC4 gene overexpression could be a prognostic factor in CRC. These results may help diagnose early-stage CRC as well as potential therapeutic targets. In summary, the integrated analysis performed herein unambiguously revealed MDK as a driver inducing the immune-tolerance phenotype in adenoma, the precancerous CRC lesion. These findings suggest that MDK signaling may play an important role in CRC progression and shows potential as an essential mediator in immunotherapeutic targeting in CRC, given its association with poor prognoses.

Contributors

M. H., Y. K., T. Shimamura, and K. M. designed the study. Y. K. and T. Shimamura directed the analysis. M. H., Y. K., and T. Shimamura performed the analysis. M. H. and T. Sakamoto conducted the experiments. All authors discussed the results. M. H. wrote the original draft of the manuscript. M. H., Y. K., and T. Shimamura have verified the underlying data. K. M., T. Shimamura, and T. Sakamoto supervised the research. All authors read and approved the final version of the manuscript.

Data sharing statement

All data reported in this paper are available from the lead contact (mimori.koshi.791@m.kyusyu-u.ac.jp) upon request. The python package of DeepCOLOR is available on Github (https://github.com/kojikoji/deepcolor) and can be directly installed. Endogenous data of the spatial transcriptomics data are stored in the DDBJ Sequence Read Archive

(DRA) (https://www.ddbj.nig.ac.jp/dra/index-e.html) and the count data are stored in the Genomic Expression Archive (GEA) (https://www.ddbj.nig.ac.jp/gea/index-e.html). The associated accession number of raw data is DRA016520 and DRA016537. The associated accession number of count data is E-GEAD-619 and E-GEAD-622. The public data analysed in this study were obtained from Gene Expression Omnibus (GEO) at GSE132465 and GSE108989.

Declaration of interests

The authors declare no competing interests.

Acknowledgements

For this study, we used the super-computing resource provided by the Human Genome Center, The Institute of Medical Science, The University of Tokyo (http://sc.hgc.jp/shirokane.html). This work was supported by the following grants and foundations: Japan Society for the Promotion of Science (JSPS) Grant-in-Aid for Science Research (grant numbers 19K09176, 19H03715, 20H05039, 20K08930, 20K17556, 20K22839, 21K07179, 22K02903, 22K09006, 22H04839, 22H0492, 23K06765, 23H04938, and 23K08074); OITA Cancer Research Foundation; AMED under Grant Number (23ck0106825h001, 23ck0106800h001, 22ama221501h0001, 22ek0109488, 22ama221215, 22ama221501, 22wm0425007, 21ck0106690s0201, 23wm0325068, 23tm0424226, 20ck0106547h0001, 20ck0106541h0001, 20cm0106475h0001, 19cm0106504h0004); Japan Science and Technology Agency (JST) (The Moonshot Moonshot R&D program, grant no. JPMJMS2025 and ACT-X program, grant no. JPMJAX20AB); Takeda Science Foundation; The Princess Takamatsu Cancer Research Fund. Further support came from the Medical Research Center Initiative for High Depth Omics and Nanken-Kyoten at Tokyo Medical and Dental University (TMDU). Supercomputing resources were provided by the Shirokane supercomputer at the Human Genome Center of the University of Tokyo, the TSUBAME3.0 supercomputer at the Tokyo Institute of Technology, and the AI Bridging Cloud Infrastructure (ABCI) at the National Institute of Advanced Industrial Science and Technology (AIST). Fig. 1a was created using bioRENDER (https://app.biorender.com/). Fig. 7e was created by EAT corporation (http://eat-inc.jp). We would like to thank Editage (https://www.editage.com/) for English language editing.

Appendix A. Supplementary data

Supplementary data related to this article can be found at https://doi.org/10.1016/j.ebiom.2024.105102.

References

1 Bray F, Ferlay J, Soerjomataram I, Siegel RL, Torre LA, Jemal A. Global cancer statistics 2018: GLOBOCAN estimates of incidence and mortality worldwide for 36 cancers in 185 countries. *CA Cancer J Clin*. 2018;68(6):394–424.
2 Lichtenstein P, Holm NV, Verkasalo PK, et al. Environmental and heritable factors in the causation of cancer–analyses of cohorts of twins from Sweden, Denmark, and Finland. *N Engl J Med*. 2000;343(2):78–85.
3 Leslie A, Carey FA, Pratt NR, Steele RJ. The colorectal adenoma-carcinoma sequence. *Br J Surg*. 2002;89(7):845–860.
4 Bond JH. Clinical evidence for the adenoma-carcinoma sequence, and the management of patients with colorectal adenomas. *Semin Gastrointest Dis*. 2000;11:176–184.
5 Corley DA, Jensen CD, Marks AR, et al. Adenoma detection rate and risk of colorectal cancer and death. *N Engl J Med*. 2014;370(14):1298–1306.
6 Brenner H, Kloor M, Pox CP. Colorectal cancer. *Lancet*. 2014;383:1490–1502.
7 Miyoshi Y, Nagase H, Ando H, et al. Somatic mutations of the APC gene in colorectal tumors: mutation cluster region in the APC gene. *Hum Mol Genet*. 1992;1(4):229–233.
8 Logan CY, Nusse R. The Wnt signaling pathway in development and disease. *Annu Rev Cell Dev Biol*. 2004;20:781–810.
9 Schatoff EM, Leach BI, Dow LE. Wnt signaling and colorectal cancer. *Curr Colorectal Cancer Rep*. 2017;13(2):101–110.
10 Cancer Genome Atlas Network. Comprehensive molecular characterization of human colon and rectal cancer. *Nature*. 2012;487(7407):330–337.
11 Fearon ER. Molecular genetics of colorectal cancer. *Annu Rev Pathol*. 2011;6:479–507.
12 Uchi R, Takahashi Y, Niida A, et al. Integrated multiregional analysis proposing a new model of colorectal cancer evolution. *PLoS Genet*. 2016;12(2):e1005778.
13 Saito T, Niida A, Uchi R, et al. A temporal shift of the evolutionary principle shaping intratumor heterogeneity in colorectal cancer. *Nat Commun*. 2018;9(1):2884.
14 Cercek A, Lumish M, Sinopoli J, et al. PD-1 blockade in mismatch repair-deficient, locally advanced rectal cancer. *N Engl J Med*. 2022;386(25):2363–2376.
15 Le DT, Uram JN, Wang H, et al. PD-1 blockade in tumors with mismatch-repair deficiency. *N Engl J Med*. 2015;372(26):2509–2520.
16 Overman MJ, McDermott R, Leach JL, et al. Nivolumab in patients with metastatic DNA mismatch repair-deficient or microsatellite instability-high colorectal cancer (CheckMate 142): an open-label, multicentre, phase 2 study. *Lancet Oncol*. 2017;18(9):1182–1191.
17 Zheng C, Zheng L, Yoo JK, et al. Landscape of infiltrating T cells in liver cancer revealed by single-cell sequencing. *Cell*. 2017;169(7):1342–1356.e16.
18 Guo X, Zhang Y, Zheng L, et al. Global characterization of T cells in non-small-cell lung cancer by single-cell sequencing. *Nat Med*. 2018;24(7):978–985.
19 Lee HO, Hong Y, Etlioglu HE, et al. Lineage-dependent gene expression programs influence the immune landscape of colorectal cancer. *Nat Genet*. 2020;52(6):594–603.
20 Ozato Y, Kojima Y, Kobayashi Y, et al. Spatial and single-cell transcriptomics decipher the cellular environment containing HLA-G+ cancer cells and SPP1+ macrophages in colorectal cancer. *Cell Rep*. 2023;42(1):111929.
21 Zheng X, Song J, Yu C, et al. Single-cell transcriptomic profiling unravels the adenoma-initiation role of protein tyrosine kinases during colorectal tumorigenesis. *Signal Transduct Target Ther*. 2022;7(1):60.
22 Becker WR, Nevins SA, Chen DC, et al. Single-cell analyses define a continuum of cell state and composition changes in the malignant transformation of polyps to colorectal cancer. *Nat Genet*. 2022;54(7):985–995.
23 Kojima Y, Mii S, Hayashi S, et al. Single-cell colocalization analysis using a deep generative model. *Cell Syst*. 2024;15(2):180–192.e7.
24 Kouyama Y, Masuda T, Fujii A, et al. Oncogenic splicing abnormalities induced by DEAD-Box Helicase 56 amplification in colorectal cancer. *Cancer Sci*. 2019;110(10):3132–3144.
25 Sato K, Masuda T, Hu Q, et al. Novel oncogene 5MP1 reprograms c-Myc translation initiation to drive malignant phenotypes in colorectal cancer. *eBioMedicine*. 2019;44:387–402.
26 Ueda M, Iguchi T, Nambara S, et al. Overexpression of transcription termination factor 1 is associated with a poor prognosis in patients with colorectal cancer. *Ann Surg Oncol*. 2015;22(Suppl 3):S1490–S1498.
27 Hamano R, Wu X, Wang Y, Oppenheim JJ, Chen X. Characterization of MT-2 cells as a human regulatory T cell-like cell line. *Cell Mol Immunol*. 2015;12(6):780–782.
28 Yoshino S, Matsui Y, Fukui Y, et al. EXOSC9 depletion attenuates P-body formation, stress resistance, and tumorigenicity of cancer cells. *Sci Rep*. 2020;10(1):9275.
29 Hara T, Nakaoka HJ, Hayashi T, et al. Control of metastatic niche formation by targeting APBA3/Mint3 in inflammatory monocytes. *Proc Natl Acad Sci U S A*. 2017;114(22):E4416–E4424.
30 Kanamori A, Matsubara D, Saitoh Y, et al. Mint3 depletion restricts tumor malignancy of pancreatic cancer cells by decreasing SKP2 expression via HIF-1. *Oncogene*. 2020;39(39):6218–6230.
31 Sakamoto T, Seiki M. Cytoplasmic tail of MT1-MMP regulates macrophage motility independently from its protease activity. *Gene Cell*. 2009;14(5):617–626.
32 Kingma DP, Welling M. Auto-encoding variational bayes. *arXiv preprint arXiv*. 2013;1312:6114.
33 Qiao W, Wang W, Laurenti E, et al. Intercellular network structure and regulatory motifs in the human hematopoietic system. *Mol Syst Biol*. 2014;10(7):741.
34 Choi H, Sheng J, Gao D, et al. Transcriptome analysis of individual stromal cell populations identifies stroma-tumor crosstalk in mouse lung cancer model. *Cell Rep*. 2015;10(7):1187–1201.
35 Ramilowski JA, Goldberg T, Harshbarger J, et al. A draft network of ligand-receptor-mediated multicellular signalling in human. *Nat Commun*. 2015;6:7866.

36 Pavličev M, Wagner GP, Chavan AR, et al. Single-cell transcriptomics of the human placenta: inferring the cell communication network of the maternal-fetal interface. *Genome Res.* 2017;27(3):349–361.
37 Browaeys R, Saelens W, Saeys Y. NicheNet: modeling intercellular communication by linking ligands to target genes. *Nat Methods.* 2020;17(2):159–162.
38 Wang Y, Wang R, Zhang S, et al. iTALK: an R Package to characterize and illustrate intercellular communication. *bioRxiv*; 2019. https://doi.org/10.1101/507871.
39 Cabello-Aguilar S, Alame M, Kon-Sun-Tack F, Fau C, Lacroix M, Colinge J. SingleCellSignalR: inference of intercellular networks from single-cell transcriptomics. *Nucleic Acids Res.* 2020;48(10):e55.
40 Hou R, Denisenko E, Ong HT, Ramilowski JA, Forrest ARR. Predicting cell-to-cell communication networks using NATMI. *Nat Commun.* 2020;11(1):5011.
41 Jin S, Guerrero-Juarez CF, Zhang L, et al. Inference and analysis of cell-cell communication using CellChat. *Nat Commun.* 2021;12(1):1088.
42 Noël F, Massenet-Regad L, Carmi-Levy I, et al. Dissection of intercellular communication using the transcriptome-based framework ICELLNET. *Nat Commun.* 2021;12(1):1089.
43 Shao X, Liao J, Li C, Lu X, Cheng J, Fan X. CellTalkDB: a manually curated database of ligand-receptor interactions in humans and mice. *Brief Bioinform.* 2021;22(4):bbaa269.
44 Page L, Brin S, Motwani R, Winograd T. *The PageRank citation ranking: bringing order to the web. Stanford Digital Library Technologies Project.* 1998. 10.1.1.31.1768.
45 Benjamini Y, Hochberg Y. Controlling the false discovery rate: a practical and powerful approach to multiple testing. *J Roy Stat Soc B.* 1996;57:289–300.
46 Zhang L, Yu X, Zheng L, et al. Lineage tracking reveals dynamic relationships of T cells in colorectal cancer. *Nature.* 2018;564(7735):268–272.
47 Li C, Jiang P, Wei S, Xu X, Wang J. Regulatory T cells in tumor microenvironment: new mechanisms, potential therapeutic strategies and future prospects. *Mol Cancer.* 2020;19(1):116.
48 Nishikawa H, Sakaguchi S. Regulatory T cells in tumor immunity. *Int J Cancer.* 2010;127(4):759–767.
49 Colombo MP, Piconese S. Regulatory-T-cell inhibition versus depletion: the right choice in cancer immunotherapy. *Nat Rev Cancer.* 2007;7(11):880–887.
50 Schaefer C, Kim GG, Albers A, Hoermann K, Myers EN, Whiteside TL. Characteristics of CD4+CD25+ regulatory T cells in the peripheral circulation of patients with head and neck cancer. *Br J Cancer.* 2005;92:913–920.
51 Ormandy LA, Hillemann T, Wedemeyer H, Manns MP, Greten TF, Korangy F. Increased populations of regulatory T cells in peripheral blood of patients with hepatocellular carcinoma. *Cancer Res.* 2005;65:2457–2464.
52 Ichihara F, Kono K, Takahashi A, Kawaida H, Sugai H, Fujii H. Increased populations of regulatory T cells in peripheral blood and tumor-infiltrating lymphocytes in patients with gastric and esophageal cancers. *Clin Cancer Res.* 2003;9:4404–4408.
53 Sasada T, Kimura M, Yoshida Y, Kanai M, Takabayashi A. CD4+CD25+ regulatory T cells in patients with gastrointestinal malignancies: possible involvement of regulatory T cells in disease progression. *Cancer.* 2003;98:1089–1099.
54 Hiraoka N, Onozato K, Kosuge T, Hirohashi S. Prevalence of FOXP3+ regulatory T cells increases during the progression of pancreatic ductal adenocarcinoma and its premalignant lesions. *Clin Cancer Res.* 2006;12:5423–5434.
55 Liyanage UK, Moore TT, Joo HG, et al. Prevalence of regulatory T cells is increased in peripheral blood and tumor microenvironment of patients with pancreas or breast adenocarcinoma. *J Immunol.* 2002;169:2756–2761.
56 Bates GJ, Fox SB, Han C, et al. Quantification of regulatory T cells enables the identification of high-risk breast cancer patients and those at risk of late relapse. *J Clin Oncol.* 2006;24:5373–5380.
57 Curiel TJ, Coukos G, Zou L, et al. Specific recruitment of regulatory T cells in ovarian carcinoma fosters immune privilege and predicts reduced survival. *Nat Med.* 2004;10:942–949.
58 Sato E, Olson SH, Ahn J, et al. Intraepithelial CD8+ tumor-infiltrating lymphocytes and a high CD8+/regulatory T cell ratio are associated with favorable prognosis in ovarian cancer. *Proc Natl Acad Sci U S A.* 2005;102(51):18538–18543.
59 Filippou PS, Karagiannis GS, Constantinidou A. Midkine (MDK) growth factor: a key player in cancer progression and a promising therapeutic target. *Oncogene.* 2020;39(10):2040–2054.
60 Cerezo-Wallis D, Contreras-Alcalde M, Troulé K, et al. Midkine rewires the melanoma microenvironment toward a tolerogenic and immune-resistant state. *Nat Med.* 2020;26(12):1865–1877.
61 Yu X, Harden K, Gonzalez LC, et al. The surface protein TIGIT suppresses T cell activation by promoting the generation of mature immunoregulatory dendritic cells. *Nat Immunol.* 2009;10(1):48–57.
62 Stanietsky N, Simic H, Arapovic J, et al. The interaction of TIGIT with PVR and PVRL2 inhibits human NK cell cytotoxicity. *Proc Natl Acad Sci U S A.* 2009;106(42):17858–17863.
63 Chauvin JM, Zarour HM. TIGIT in cancer immunotherapy. *J Immunother Cancer.* 2020;8(2):e000957.
64 Guo H, Jin D, Chen X. Lipocalin 2 is a regulator of macrophage polarization and NF-κB/STAT3 pathway activation. *Mol Endocrinol.* 2014;28(10):1616–1628.
65 Swigris JJ, Brown KK. The role of endothelin-1 in the pathogenesis of idiopathic pulmonary fibrosis. *BioDrugs.* 2010;24(1):49–54.
66 Ito TK, Ishii G, Chiba H, Ochiai A. The VEGF angiogenic switch of fibroblasts is regulated by MMP-7 from cancer cells. *Oncogene.* 2007;26(51):7194–7203.
67 Lee HT, Liu SP, Lin CH, et al. A crucial role of CXCL14 for promoting regulatory T cells activation in stroke. *Theranostics.* 2017;7(4):855–875.
68 Chang AL, Miska J, Wainwright DA, et al. CCL2 produced by the glioma microenvironment is essential for the recruitment of regulatory T cells and myeloid-derived suppressor cells. *Cancer Res.* 2016;76(19):5671–5682.
69 Jin J, Lin J, Xu A, et al. CCL2: an important mediator between tumor cells and host cells in tumor microenvironment. *Front Oncol.* 2021;11:722916.
70 Patterson SJ, Pesenacker AM, Wang AY, et al. T regulatory cell chemokine production mediates pathogenic T cell attraction and suppression. *J Clin Invest.* 2016;126(3):1039–1051.
71 Zhang Y, Zuo C, Liu L, et al. Single-cell RNA-sequencing atlas reveals an MDK-dependent immunosuppressive environment in ErbB pathway-mutated gallbladder cancer. *J Hepatol.* 2021;75(5):1128–1141.
72 Ye C, Qi M, Fan QW, et al. Expression of midkine in the early stage of carcinogenesis in human colorectal cancer. *Br J Cancer.* 1999;79(1):179–184.
73 Kemper M, Hentschel W, Graß JK, et al. Serum Midkine is a clinical significant biomarker for colorectal cancer and associated with poor survival. *Cancer Med.* 2020;9(6):2010–2018.
74 Dunn GP, Old LJ, Schreiber RD. The immunobiology of cancer immunosurveillance and immunoediting. *Immunity.* 2004;21(2):137–148.
75 Ergüven M, Muramatsu T, Bilir A. *Midkine: from embryogenesis to pathogenesis and therapy.* Springer Science & Business Media; 2012.
76 Deepa SS, Yamada S, Zako M, Goldberger O, Sugahara K. Chondroitin sulfate chains on syndecan-1 and syndecan-4 from normal murine mammary gland epithelial cells are structurally and functionally distinct and cooperate with heparan sulfate chains to bind growth factors. A novel function to control binding of midkine, pleiotrophin, and basic fibroblast growth factor. *J Biol Chem.* 2004;279(36):37368–37376.
77 Zhu Y, Zheng D, Lei L, et al. High expression of syndecan-4 is related to clinicopathological features and poor prognosis of pancreatic adenocarcinoma. *BMC Cancer.* 2022;22(1):1042.
78 Jechorek D, Haeusler-Pliske I, Meyer F, Roessner A. Diagnostic value of syndecan-4 protein expression in colorectal cancer. *Pathol Res Pract.* 2021;222:153431.
79 Poças J, Marques C, Gomes C, et al. Syndecan-4 is a maestro of gastric cancer cell invasion and communication that underscores poor survival. *Proc Natl Acad Sci U S A.* 2023;120(20):e2214853120.
80 Yang H, Liu Y, Zhao MM, et al. Therapeutic potential of targeting membrane-spanning proteoglycan SDC4 in hepatocellular carcinoma. *Cell Death Dis.* 2021;12(5):492.
81 Saoncella S, Echtermeyer F, Denhez F, et al. Syndecan-4 signals cooperatively with integrins in a Rho-dependent manner in the assembly of focal adhesions and actin stress fibers. *Proc Natl Acad Sci U S A.* 1999;96(6):2805–2810.

82 Bass MD, Morgan MR, Humphries MJ. Integrins and syndecan-4 make distinct, but critical, contributions to adhesion contact formation. *Soft Matter*. 2007;3(3):372–376.

83 Mostafavi-Pour Z, Askari JA, Parkinson SJ, Parker PJ, Ng TT, Humphries MJ. Integrin-specific signaling pathways controlling focal adhesion formation and cell migration. *J Cell Biol*. 2003;161(1):155–167.

84 Jeyarajah MJ, Jaju Bhattad G, Kops BF, Renaud SJ. Syndecan-4 regulates extravillous trophoblast migration by coordinating protein kinase C activation. *Sci Rep*. 2019;9(1):10175.

85 Becsky D, Szabo K, Gyulai-Nagy S, et al. Syndecan-4 modulates cell polarity and migration by influencing centrosome positioning and intracellular calcium distribution. *Front Cell Dev Biol*. 2020;8:575227.

86 Reynolds PR, Mucenski ML, Le Cras TD, Nichols WC, Whitsett JA. Midkine is regulated by hypoxia and causes pulmonary vascular remodeling. *J Biol Chem*. 2004;279(35):37124–37132.

87 Tang SL, Gao YL, Chen XB. Wnt/β-catenin up-regulates Midkine expression in glioma cells. *Int J Clin Exp Med*. 2015;8(8):12644–12649.

88 Ge Z, Peppelenbosch MP, Sprengers D, Kwekkeboom J. TIGIT, the next step towards successful combination immune checkpoint therapy in cancer. *Front Immunol*. 2021;12:699895.